A THEORETICAL INVESTIGATION OF THE ELECTRONIC BAND STRUCTURE AND BULK PROPERTIES OF DIAMOND

By

RICHARD ALAN HEATON

Bachelor of Science

Oklahoma State University

Stillwater, Oklahoma

1972

Submitted to the Faculty of the Graduate College
of the Oklahoma State University
in partial fulfillment of the requirements
for the Doctor of
DOCTOR OF PHILOSOPHY
May, 1979

A THEORETICAL INVESTIGATION OF THE

ELECTRONIC BAND STRUCTURE AND

BULK PROPERTIES OF DIAMOND

Thesis Approved:

Earl E Lafon
Thesis Adviser

Inder Paul Batra

Paul Westhaus

Timothy M Wilson

Richard C Powell

Norman N Durham
Dean of the Graduate College

PREFACE

This study is primarily concerned with demonstrating the accuracy and ease with which the method of linear combination of atomic orbitals (LCAO) is able to calculate bulk crystal properties. The great versatility of the representation of the crystal obtained with this method gives it widespread applicability to all areas of crystal related problems.

The author wishes to express his appreciation to his major adviser, Dr. Earl Lafon, for his invaluable assistance with the formulations and his unfailing guidance throughout this study. Appreciation is extended to a committee member Dr. Inder Batra for his guidance during one summer at IBM Research Labs in San Jose, California. Appreciation is also extended to other committee members, Dr. Paul Westhaus, Dr. Tim Wilson and Dr. Richard Powell, for their support and guidance during this study.

The author is grateful to his wife, Irene, for her assistance in typing earlier copies of this manuscript and for her support throughout this investigation. Thanks is also extended to Janet Sallee for the excellence of the final copy. In addition, appreciation is extended to the Research Foundation at Oklahoma State University for their very generous donation of computer funds. This work was also supported in part by a Contract No. F33615-71-C-1395 issued by the Aerospace Research Laboratory, Air Force Systems Command, U.S. Air Force, Wright-Patterson AFB, Ohio.

TABLE OF CONTENTS

LIST OF TABLES

LIST OF FIGURES

CHAPTER I

INTRODUCTION

The calculation of the electronic properties of crystals has always been of great interest to solid state physicists. The symmetry properties of crystals when correctly utilized enable an accurate representation of the entire crystal within the limitations of an independent particle model. Many techniques have been developed to obtain this representation such as the orthogonalized-plane-wave (OPW) (1) method, Green's-function (KKR) (2,3) method, and linear combination of atomic orbitals (LCAO) (4).

The method of LCAO was originally proposed by Bloch (3) in 1928. It was initially introduced under the name tight binding and as the name suggests rather severe approximations were adopted. Because of the difficulty in evaluating the required multicenter integrals, the lattice sums were truncated at first nearest neighbor. This turned out to be an unphysical approximation and as a result tight binding gained a bad reputation in the scientific community. It was not until a historic paper by Lafon and Lin (4) in 1966 that tight binding was extended into the method of LCAO for which the lattice sums are carried to convergence. Their breakthrough was made possible by the advent of modern computers and the formulation of the multicenter integrals in terms of reciprocal space.

In this investigation a self-consistent Hartree-Fock-Slater calcu-

lation for diamond will be performed using the method of LCAO (4,5). The objectives of this study will be many-fold. A primary objective is to obtain an accurate self-consistent representation of diamond and compare the resulting band structure with reliable experimental measurements. However, band structure is difficult to verify experimentally. There are only a few qualitative features of the band structure for which a direct comparison with experiment is possible: such as, indirect band gap, location of the minimum of the conduction band and valence band width. Beyond this limited analysis and some simple symmetry checks, little else can be verified about the band structure. Additionally, band structure is only an indication of band state energies in the Brillouin zone along high symmetry lines. It does not test the band state energies throughout the volume of the Brillouin zone. More importantly, examination of band structure reveals little about the more sensitive wavefunctions.

A valid evaluation of a self-consistent calculation would be to use the wavefunctions to predict bulk properties already measured experimentally. The resulting direct comparison between theory and experiment would test the wavefunctions throughout the Brillouin zone. Two ground state properties of diamond for which experimental results already exist are x-ray structure factors and Compton profile. Another objective of this study then is the accurate evaluation of x-ray structure factors and Compton profiles from the self-consistent wavefunctions.

The choice of diamond as the candidate of study was made because of the many interesting properties it possesses. Diamond is unique from a theoretical point of view because its covalent bonds are well

defined (6). The covalent bond model is very important in understanding a great many substances, such as silicon and other group-IV materials. Also, diamond is interesting because it has a small core. Not only does this reduce the computational complexity, but more importantly, the core states do not tend to dominate the bulk properties. Two-thirds of diamond's electrons participate in the valence band. Furthermore, a recent self-consistent Hartree-Fock calculation using the method of LCAO (18,23) was completed for diamond. Self-consistent Hartree-Fock calculations have been done for very few materials, so a direct comparison between these two theoretical approaches would be very enlightening.

The LCAO method has been applied self-consistently within the Hartree-Fock-Slater formulation for both metals (7) and insulators (8). In this investigation, the desire for a large degree of variational freedom will be balanced by the need to evaluate the wavefunctions and bulk properties using a large number of low symmetry points throughout the Brillouin zone. A generalized method of optimized orbitals which provides adequate variational freedom while maintaining a small basis set will be introduced. The calculation is carried to self-consistency while allowing the optimized orbital basis set to relax with each iteration. The bulk properties are calculated from the self-consistent wavefunctions and special emphasis is placed on the comparison of ground state properties with experiment.

CHAPTER II

LCAO APPLIED TO DIAMOND

A. Crystal Symmetry

The diamond symmetry consists of two interpenetrating face-centered-cubic lattices (fcc) which will be referred to as sublattice one and two. Each sublattice has the same lattice constant a_o chosen to be 6.728 a.u. These two periodic arrays of atoms are identically aligned but offset from each other by a non-primitive translation of one fourth the distance along the main diagonal of the fcc unit cell. For convenience, the origin is placed on this diagonal midway between the atom sites corresponding to an inversion point of the crystal. The coordinates of the carbon atoms so arranged are given by

$$\vec{T}_{vi} = \vec{R}_v + \vec{t}_i; \; i = 1,2,$$

where

$$\vec{t}_1 = -a_o(1,1,1)/8 = -\vec{t}_2, \tag{2.1}$$

$$\vec{R}_v = v_1\vec{a}_1 + v_2\vec{a}_2 + v_3\vec{a}_3,$$

and where v_1, v_2, v_3 are integers. The primitive lattice vectors $\vec{a}_1$, $\vec{a}_2$, $\vec{a}_3$ are chosen to be

$$\vec{a}_1 = a_o(1,-1,0)/2,$$

$$\vec{a}_2 = a_o(0,1,-1)/2, \qquad (2.2)$$

$$\vec{a}_3 = a_o(0,0,1) .$$

The Wigner-Seitz cell constructed about the origin contains two atoms with positions given by $\vec{t}_1$ and $\vec{t}_2$. It has a volume Ω equal to $a_o^3/4$. Every point outside this volume is related to some point inside by a translation vector $\vec{R}_v$.

The reciprocal lattice is derived from the primitive lattice vectors and is body-centered-cubic (bcc) with lattice vectors $\vec{K}_v$ given by

$$\vec{K}_v = v_1\vec{b}_1 + v_2\vec{b}_2 + v_3\vec{b}_3 \qquad (2.3)$$

where

$$\vec{b}_1 = 2\pi(2,0,0)/a_o,$$

$$\vec{b}_2 = 2\pi(2,2,0)/a_o, \qquad (2.4)$$

$$\vec{b}_3 = 2\pi(1,1,1)/a_o.$$

The Brillouin zone (BZ) centered about the origin in reciprocal space contains one lattice point and has a volume Ω_k with the magnitude $(2\pi)^3/\Omega$. It is always possible to write some general point $\vec{\kappa}$ in reciprocal space as a sum $\vec{k} + \vec{K}_v$, where $\vec{k}$ lies within this volume or on the boundary.

The rotation-reflection symmetry of the direct lattice together with the translation group forms a non-symmorphic space group which has

the point group symmetry O_h. In this investigation extensive use will be made of rotation-reflection symmetry in order to eliminate redundant calculations. In the Brillouin zone the wavefunctions and eigenvalues are calculated directly in a fundamental segment called the irreducible wedge (IW) with a volume equal to $\Omega_k/48$. The irreducible wedge has the property that it reproduces the entire Brillouin zone when operated on by the 48 rotation-reflection operations of O_h. By utilizing this symmetry, wavefunctions everywhere in the Brillouin zone can be related to wavefunctions calculated in the wedge. The irreducible wedge chosen in this investigation consists of all the points

$$\vec{\kappa} = k_1\vec{b}_1 + k_2\vec{b}_2 + k_3\vec{b}_3$$

which lie in the Brillouin zone and for which k_1, k_2 and k_3 are greater than and equal to zero.

In the Wigner-Steiz cell a similar fundamental segment exists called the irreducible volume (IV) with the volume $\Omega/48$. The form of this volume is slightly more complicated because of the glide plane symmetry and is given in Appendix B. By utilizing the space group symmetry it is possible to generate band state wavefunctions throughout the crystal from knowledge of wavefunctions within the irreducible volume.

B. Band State Hamiltonian

Application of the Hartree-Fock-Slater (9) formulation reduces the many-body crystal Hamiltonian to a one electron model Hamiltonian resulting in the following Schrödinger equation

$$\left[-\frac{1}{2}\nabla^2 + V(\vec{r})\right]\psi_{n,i}(\vec{k},\vec{r}) = E_n(\vec{k})\psi_{n,i}(\vec{k},\vec{r}) \tag{2.5}$$

for any point $\vec{k}$ of interest in the Brillouin zone. The energy $E_n(\vec{k})$ of the nth band and the corresponding wavefunctions $\psi_{n,i}(\vec{k},\vec{r})$ with degeneracy label i are obtained from solution of the previous equation. The potential energy $V(\vec{r})$ is the sum of two terms

$$V(\vec{r}) = V_{coul}(\vec{r}) + V_{ex}(\vec{r}), \tag{2.6}$$

where $V_{coul}(\vec{r})$ is the coulomb potential obtained from solution of Poisson's equation and $V_{ex}(\vec{r})$ is the effective Slater exchange potential. Both the coulomb and exchange potentials are written in terms of the absolute value of electronic charge density $\rho(\vec{r})$ as

$$\nabla^2 V_{coul}(\vec{r}) = 4\pi Z_c \sum_{\nu}\sum_{i} \delta(\vec{r}-\vec{T}_{\nu i}) - 4\pi\rho(\vec{r}) \tag{2.7}$$

and

$$V_{ex}(\vec{r}) = -\frac{3}{2}(3/\pi)^{1/3}\rho^{1/3}(\vec{r}), \tag{2.8}$$

where Z_c is the atomic number of carbon and $\rho^{1/3}(\vec{r})$ is the positive cube root of electronic charge density evaluated at $\vec{r}$.

Since the crystal potential and the charge density have the periodicity of the crystal, it is possible and convenient to re-express them in a Fourier series expanded about the origin as

$$V(\vec{r}) = \sum_{\nu}(V_{coul}(\vec{K}_\nu) + V_{ex}(\vec{K}_\nu)\cos\vec{K}_\nu\cdot\vec{r} \tag{2.9}$$

and

$$\rho(\vec{r}) = \sum_{\nu} \rho(\vec{K}_{\nu}) \cos \vec{K}_{\nu} \cdot \vec{r} \ . \tag{2.10}$$

The Fourier coefficients of both series are real because of the inversion symmetry at the origin and are given by

$$V_{coul}(\vec{K}_{\nu}) = \frac{1}{n\Omega} \int_{n\Omega} V_{coul}(\vec{r}) \cos \vec{K}_{\nu} \cdot \vec{r} \, d\tau_r, \tag{2.11}$$

$$V_{ex}(\vec{K}_{\nu}) = \frac{1}{n\Omega} \int_{n\Omega} V_{ex}(\vec{r}) \cos \vec{K} \cdot \vec{r} \, d\tau_r \tag{2.12}$$

and

$$\rho(\vec{K}_{\nu}) = \frac{1}{n\Omega} \int_{n\Omega} \rho(\vec{r}) \cos \vec{K}_{\nu} \cdot \vec{r} \, d\tau_r, \tag{2.13}$$

where n represents, symbolically, the number of unit cells in the crystal.

The LCAO approach used in this investigation will deal directly with the Fourier coefficients of crystal potential. By transforming both sides of Eqn. 2.7 into a Fourier representation, Poisson's equation can readily be solved resulting in

$$K_{\nu}^2 V_{coul}(\vec{K}_{\nu}) = - 4\pi[(2Z_c/\Omega) \cos \vec{K}_{\nu} \cdot \vec{t}_1 - \rho(\vec{K}_{\nu})] \ . \tag{2.14}$$

In a similar manner, an expression for Fourier coefficients of the exchange potential is easily obtained and written as

$$V_{ex}(\vec{K}_{\nu}) = - \frac{3}{2}(3/\pi)^{1/3} \rho^{1/3}(\vec{K}_{\nu}), \tag{2.15}$$

where $\rho^{1/3}(\vec{K}_{\nu})$ is the Fourier coefficient of $\rho^{1/3}(\vec{r})$. It is therefore possible to obtain the crystal potential directly from knowledge of the

charge density.

C. LCAO Method

In the LCAO approach to crystals, basis functions are comprised of orbitals centered on each atom site and combined together to satisfy the Bloch condition. Two different types of orbitals are used in this investigation. The first type consists entirely of single Gaussians and forms a basis set containing 112 Bloch functions. The second type of orbital used here is a linear combination of single Gaussians called an optimized orbital and it forms a basis set containing 18 Bloch functions. Obviously, the second type of orbital is more attractive because of the difference in the size of the basis sets. The details of the formation of an optimized orbital basis set will be left to a later section and we will consider only the first basis set for now. It is trivial to extend the formulation that follows to a contracted Gaussian basis set.

A straightforward choice for the single Gaussian Bloch sums is of the form

$$b^{i}_{\alpha,j}(\vec{k},\vec{r}) = n^{-\frac{1}{2}} \sum_{\nu} e^{i\vec{k}\cdot\vec{R}_{\nu}} \chi_{\alpha}(\beta_j,\vec{r}-\vec{R}_{\nu}-\vec{t}_i), \tag{2.16}$$

where

$$\alpha = s, P_x, P_y, P_z; \; i = 1,2,$$

and where the Gaussian orbitals $\chi_{\alpha}(\beta,\vec{r})$ are given by

$$\chi_s(\beta,\vec{r}) = e^{-\beta r^2}, \tag{2.17}$$

$$\chi_{P_x}(\beta,\vec{r}) = Xe^{-\beta r^2} . \qquad (2.18)$$

However, a large simplication can be made by choosing an alternative but equally valid functional form. It is obtained by taking + and - combinations of Eqn. 2.16 and introducing a phase FACTOR I_α^Δ resulting in the final expression

$$b_{\alpha,j}^{\Delta}(\vec{k},\vec{r}) = n^{-\frac{1}{2}} I_\alpha^\Delta \sum_\nu e^{i\vec{k}\cdot\vec{R}_\nu} \chi_\alpha^{-\Delta}(\beta_j, \vec{r}-\vec{R}_\nu), \qquad (2.19)$$

where

$$\Delta = +, - ;$$

$$I_\alpha^+ = -iI_\alpha^- = \begin{cases} 1 \text{ for } \alpha = s \\ i \text{ for } \alpha = P_x, P_y, P_z \end{cases}$$

and where $\bar{X}_\alpha^\Delta$ is a linear superposition of orbitals centered at $\vec{t}_1$ and $\vec{t}_2$ given by

$$\bar{X}_\alpha^\Delta(\beta,\vec{r}) = X_\alpha(\beta,\vec{r}-\vec{t}_1) + \Delta\chi_\alpha(\beta,\vec{r}-\vec{t}_2). \qquad (2.20)$$

The set of Gaussian exponents β used in this calculation were obtained from Huizinga (10) for the free carbon atom and are 4232.61, 634.882, 146.097, 42.4974, 18.1557, 14.1892, 5.14773, 3.9864, 1.96655, 1.14293, 0.49624, 0.35945, 0.15331, and 0.1146. The use of exponents from an atomic calculation should give sufficient variational freedom in a crystal calculation since contracted atomic orbitals basis sets give reasonable band structure (11). It seems justified then to assume that adequate relaxation of the crystalline wavefunctions can be obtained,

while keeping the atomic exponential set intact. This is particularly true in a decontracted calculation composed only of single Gaussians for which an exceptionally large amount of variational freedom would be expected.

The wavefunctions which satisfy Eqn. 2.5 will be linear combinations of the basis functions, where the linear coefficients are calculated by applying the method of linear variation of parameters. By employing this variational procedure two things are guaranteed, (1) the band energies are absolute minimums in energy for the given variational basis and (2) the true energy values for given Hamiltonian are lower bounds to the calculated band energies. Using the Bloch basis $b^{\Delta}_{\alpha,j}(\vec{k},\vec{r})$, the wavefunctions $\psi_{n,i}(\vec{k},\vec{r})$ and associated band energies $E_n(\vec{k})$ for the nth band at a particular point $\vec{k}$ in the Brillouin zone are obtained from solutions of the matrix equation

$$[H(\vec{k}) - E_n(\vec{k})\, S(\vec{k})]\, \vec{a}(n,i|\vec{k}) = 0 \qquad (2.21)$$

and the orthonormality condition

$$\int_{n\Omega} \psi^{*}_{n',i'}(\vec{k},\vec{r})\, \psi_{n,i}(\vec{k},\vec{r})\, d\tau_r = \delta_{nn'}\delta_{ii'},$$

where the $\psi_{n,i}(\vec{k},\vec{r})$ are given in terms of the eigenvectors $\vec{a}(n,i|\vec{k})$ by

$$\psi_{n,i}(\vec{k},\vec{r}) = \sum_{\alpha}\sum_{\Delta}\sum_{j} a^{\Delta}_{\alpha,j}(n,i|\vec{k})\, b^{\Delta}_{\alpha,j}(\vec{k},\vec{r}) \; . \qquad (2.22)$$

Normally the matrix components of $H(\vec{k})$ and $S(\vec{k})$ are complex numbers. However, the choice of Bloch function $b^{\Delta}_{\alpha,j}(\vec{k},\vec{r})$, because of the inversion symmetry at the origin, results in real matrix elements given by

$$H^{\Delta\Delta'}_{\alpha,j;\alpha',j'}(\vec{k}) = \int_{n\Omega} b^{\Delta*}_{\alpha,j}(\vec{k},\vec{r}) \left[-\frac{1}{2}\nabla^2 + V(\vec{r})\right] b^{\Delta'}_{\alpha',j'}(\vec{k},\vec{r})\, d\tau_r, \quad (2.23)$$

$$S^{\Delta\Delta'}_{\alpha,j;\alpha',j'}(k) = \int_{n\Omega} b^{\Delta*}_{\alpha,j}(\vec{k},\vec{r})\, b^{\Delta'}_{\alpha',j'}(\vec{k},\vec{r})\, d\tau_r \,. \quad (2.24)$$

The only case for which non-trivial normalizable solutions to Eqn. 2.21 exist is if

$$\det\left|H(\vec{k}) - E(\vec{k})\, S(\vec{k})\right| = 0 \,. \quad (2.25)$$

This is called a secular equation and is evaluated to obtain the band energies $E_n(\vec{k})$.

As mentioned previously, rotational symmetry can be used to optimize the computation of wavefunctions and associated bulk properties. If R_γ is a member of O_h and $\vec{\tau}_\gamma$ is the corresponding non-symmorphic translation, symmetry demands that

$$V(R_\gamma\vec{r} + \vec{\tau}_\gamma) = V(\vec{r}) \quad (2.26)$$

and

$$\rho(R_\gamma\vec{r} + \vec{\tau}_\gamma) = \rho(\vec{r}) \quad (2.27)$$

and the wavefunctions and band energies must transform like

$$E_n(R_\gamma\vec{k}) = E_n(\vec{k}) \quad (2.28)$$

and

$$\psi_{n,i}(R_\gamma\vec{k},\ R_\gamma\vec{r} + \vec{\tau}_\gamma) = \sum_j C^n_{ij}(\gamma,\vec{k})\, \psi_{n,j}(\vec{k},\vec{r}) \,. \quad (2.29)$$

These relations can in turn be used to show that the eigenvectors

$\vec{a}(n,i|R_\gamma\vec{k})$ at points outside the irreducible wedge are related to eigenvectors $\vec{a}(n,i|\vec{k})$ within the irreducible wedge by

$$\vec{a}(n,i|R_\gamma\vec{k}) = U(\gamma,\vec{k})\vec{a}(n,i|\vec{k}). \tag{2.30}$$

Both matices $C^n(\gamma,\vec{k})$ and $U(\gamma,\vec{k})$ represent unitary transformations and their explicit derivation for the diamond structure is done in Appendix A. By correct utilization of these symmetry properties integrations over all real space (reciprocal space) can be transformed into a sum of integrations over the irreducible volume (irreducible wedge).

D. Self-Consistent LCAO

Since the wavefunctions which form solutions to matrix Eq. 2.21 generally produce a charge density which is not consistent with original estimates of the crystal potential, an iterative procedure is necessary to reach internal consistency. The starting or zeroth iteration potential is generated from the absolute value of electronic charge density $\rho^o(\vec{r})$, where the superscript denotes the iteration. In this investigation, $\rho^o(\vec{r})$ was generated from superposition of the electronic portion of the atomic charge densities centered on each atom site. This can be written formally as

$$\rho^o(\vec{r}) = \sum_v \sum_i \rho_{ATOM}(\vec{r} - \vec{T}_{vi}), \tag{2.31}$$

where $\rho_{ATOM}(\vec{r})$ is the electronic charge density associated with a free carbon atom. The charge density $\rho_{ATOM}(\vec{r})$ has spherical symmetry, so the Fourier coefficients of $\rho^o(\vec{r})$ are given by

$$\rho^o(\vec{K}_v) = \frac{8\pi}{\Omega}\cos \vec{K}_v\cdot\vec{t}_1 \int_o^\infty \rho_{ATOM}(r)j_o(K_v r)r^2 dr\ . \tag{2.32}$$

The Fourier coefficients $\rho^{1/3}(\vec{K}_v)$ must be calculated numerically and the procedure is the same as outlined in Chapter III. The Fourier coefficients $\rho^{o}(\vec{K}_v)$ and $\rho^{1/3}(\vec{K}_v)$ are then substituted into Eq. 2.14 and Eq. 2.15 from which the zeroth iteration crystal potential $V^{o}(\vec{K}_v)$ is obtained. The initial potential is used to construct the matrix Eq. 2.21 which is solved to obtain the zeroth order wavefunctions $\psi^{o}_{n,i}(\vec{k},\vec{r})$ and band energies $E^{o}_{n}(\vec{k})$. The first iteration charge density $\rho'(\vec{r})$ is calculated from the wavefunctions $\psi^{o}_{n,i}(\vec{k},\vec{r})$ and used to create a first iteration potential $V'(\vec{K}_v)$. This procedure is continued for as many iterations as necessary to reach convergence. Self-consistency is obtained when the charge density $\rho^{\lambda+1}(\vec{r})$ is consistent with the potential $V^{\lambda}(\vec{r})$ from which it was generated. A convergence stabilizing technique (12) is employed for the first few iterations until the $\rho^{\lambda}(\vec{K}_v)$ have converged to at least three significant figures.

A self-consistent crystal calculation generally involves many iterations. In each iteration charge density must be evaluated which requires an integration over the Brillouin zone. This integration is done numerically over an evenly spaced mesh of 912 points (19 points in the irreducible wedge). At each of these points eigenvalues and eigenvectors must be generated. This requires the solution of a large secular equation (112 x 112) for the 19 irreducible wedge mesh points. Many numerical difficulties such as linear dependency can make the evaluation of a secular matrix constructed from a large single Gaussian basis set very difficult. Such a large basis set is also very expensive in terms of the amount of computational effort required. However, a single Gaussian basis set does provide a high degree of variational freedom for all the bands of interest at every $\vec{k}$ point. A more flexi-

ble approach would be to incorporate the variational freedom of a large single Gaussian basis set into a small manageable basis set.

It has already been demonstrated (24) that optimized orbitals are capable of providing considerable accuracy while limiting the size of the basis set to a small number of contracted Gaussian orbitals. Also, the accuracy of the results of an investigation can be enhanced by the proper selection of this contracted basis set. The method of optimized orbitals used in this problem is a two step process. The first step employs the general single Gaussian basis set described previously in a straightforward calculation of eigenvectors and eigenvalues at selected high symmetry points in the Brillouin zone. Optimized orbitals are projected out of the eigenvectors obtained in this initial step. The second phase utilizes a basis set comprised of a selection of these optimized orbitals. This new projected set of orbitals is then used for the rest of the iteration.

The technique used to form the optimized orbitals is best described by rewriting Eq. 2.22 as

$$\psi_{n,i}(\vec{k},\vec{r}) = \eta^{-\frac{1}{2}} \sum_{v} e^{i\vec{k}\cdot\vec{R}_v} \sum_{\alpha} \sum_{\Delta} I_{\alpha}^{\Delta} \Phi_{\alpha}^{\Delta}(n,i|\vec{k},\vec{r}-\vec{R}_v), \tag{2.33}$$

where

$$\bar{\phi}_{\alpha}^{\Delta}(n,i|\vec{k},\vec{r}) = \phi_{\alpha\Delta'}(n,i|\vec{k},\vec{r}-\vec{t}_1) + \Delta\phi_{\alpha\Delta'}(n,i|\vec{k},\vec{r}-\vec{t}_2)$$

The orbitals $\phi_{\alpha\Delta'}(n,i|\vec{k},\vec{r})$ are called optimized orbitals and are given by

$$\phi_{\alpha\Delta'}(n,i|\vec{k},\vec{r}) = \sum_{j} a_{\alpha j}^{\Delta'}(n,i|\vec{k})\, X_{\alpha}(\beta_j,\vec{r}) \tag{2.34}$$

The contraction coefficients $a^{\Delta'}_{\alpha j}(n,i|\vec{k})$ are the associated eigenvector coefficients obtained using the original Gaussian basis set.

The main criterion used in selecting an optimized orbital basis set is that it should adequately represent all the band states of interest. One of the reasons why a small basis set is able to satisfy this requirement so well is that in group IV materials the bonds are reasonably well defined and maintain their integrity throughout the Brillouin zone. With this in mind, the optimized basis set is formed from states from the top, middle and bottom of the valence band. During the iterative phase of this calculation, since we are primarily interested in occupied bands, no optimized orbitals from the conduction band are included in the basis set. However, the optimized orbitals taken from the top of the valence band are close enough in energy to the bottom portion of the conduction band to provide variational freedom for lower lying conduction states. As a result reasonably good lower lying conduction bands are obtained without any additional optimized orbitals. The optimized basis set used for the λth iteration is

$$\phi_1^{\lambda}(\vec{r}) = \phi_{s+}^{\lambda}(1,1|\Gamma,\vec{r}), \text{ (core state at } \Gamma)$$

$$\phi_2^{\lambda}(\vec{r}) = \phi_{s+}^{\lambda}(3,1|\Gamma,\vec{r}), \text{ (bottom of valence band at } \Gamma)$$

$$\phi_3^{\lambda}(\vec{r}) = \phi_{s+}^{\lambda}(3,1|X,\vec{r}), \text{ (bottom of valence band at X)}$$

$$\phi_4^{\lambda}(\vec{r}) = \phi_{p_x-}(3,1|X,\vec{r}), \text{ (bottom of valence band at X)}$$

$$\phi_5^{\lambda}(\vec{r}) = \phi_{p_x-}(4,1|\Gamma,\vec{r}), \text{ (top of valence band at } \Gamma)$$

$$\phi_6^\lambda(\vec{r}) = y\,\phi_4^\lambda(\vec{r})/X, \qquad \phi_7^\lambda(\vec{r}) = y\,\phi_5^\lambda(\vec{r})/X\ ,$$

$$\phi_8^\lambda(\vec{r}) = z\,\phi_4^\lambda(\vec{r})/X, \qquad \phi_9^\lambda(\vec{r}) = z\,\phi_5^\lambda(\vec{r})/X\ . \tag{2.35}$$

As mentioned previously, a new set of optimized orbitals are formed for each successive iteration from the original single Gaussian basis set. This is desirable because small changes in the potential will result in a slightly different optimized orbital basis set and reoptimizing the orbitals allows them to relax to the new crystalline environment. A typical example of the effect of this relaxation is shown in Figure 1 for ϕ_5 between the initial and the final iteration. This figure also contrasts the difference between an atomic ϕ_{p_x} orbital and the optimized ϕ_5 orbitals. This clearly illustrates the improvements possible by employing an optimized basis set rather than a purely atomic basis set for representing the band state wavefunctions.

The variational wavefunction can now be written in terms of the optimized Gaussian orbitals for the λth iteration as

$$\psi_{n,i}^\lambda(\vec{k},\vec{r}) = \sum_j \sum_\Delta A_j^{\lambda\Delta}(n,i|\vec{k})\, B_j^{\lambda\Delta}(\vec{k},\vec{r}) \tag{2.36}$$

$$= \eta^{-\frac{1}{2}} \sum_\nu e^{i\vec{k}\cdot\vec{R}_\nu}\, \xi_{n,i}^\lambda(\vec{k},\vec{r}-\vec{R}_\nu) \tag{2.37}$$

where

$$B_j^{\lambda\Delta}(\vec{k},\vec{r}) = \eta^{-\frac{1}{2}}\, I_j^\Delta \sum_\nu e^{i\vec{k}\cdot\vec{R}_\nu} \left[\phi_j^\lambda(\vec{r}-\vec{R}_\nu-\vec{t}_1) + \Delta\phi_j^\lambda(\vec{r}-\vec{R}_\nu-\vec{t}_2)\right] \tag{2.38}$$

and

$$\xi_{n,i}^\lambda(\vec{k},\vec{r}) = \sum_\Delta \sum_j I_j^\Delta\, A_j^{\lambda\Delta}(n,i|\vec{k})\left[\phi_j^\lambda(\vec{r}-\vec{t}_1) + \Delta\phi_j^\lambda(\vec{r}-\vec{t}_2)\right] \tag{2.39}$$

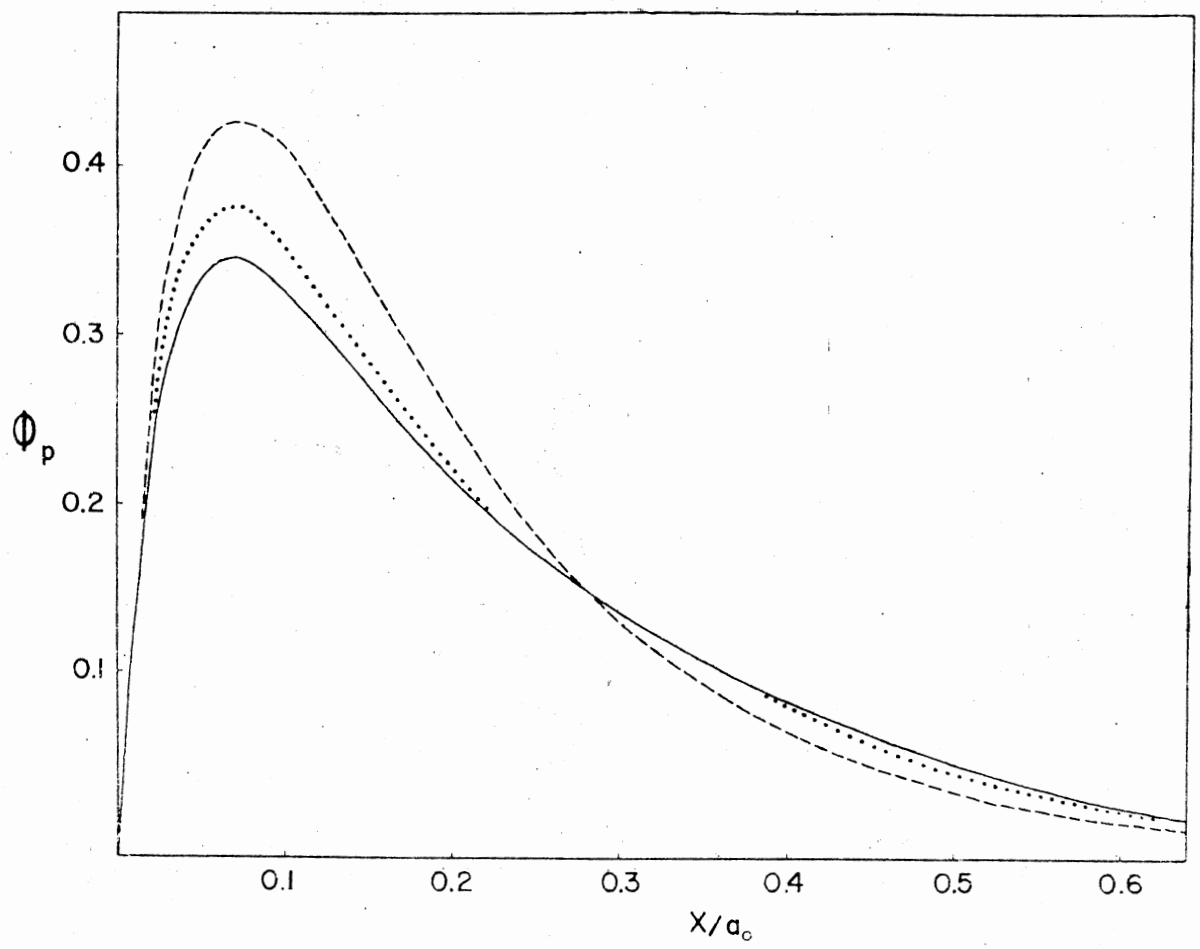

Figure 1. Illustration of Relaxation of Optimized Orbitals to the Crystalline Potential. The dashed curve is the atomic 2p orbital, the dotted (solid) curve is the p-orbital from top of valence band at Γ-point as obtained during the first (last) iteration

and where $A_j^{\lambda\Delta}(n,i|\vec{k})$ are the eigenvector coefficients obtained from solution of the appropriate secular equation.

The final self-consistent band structure for diamond is presented in Figure 2. Since it is desirable to enhance the accuracy of the lower lying conduction bands additional optimized orbitals are taken from the bottom of the conduction band at X. These orbitals together with ϕ_5, ϕ_7 and ϕ_9 should provide adequate variational flexability for the conduction states. In this context, we are interested in seeing what lower lying conduction states are predicted from a self-consistent charge density. The band structure predicts an indirect band gap of 5.2 ev which is in excellent agreement with the experimental value of 5.4 ev (13). The associated minimum of the conduction band is calculated to lie at $2\pi(0.68,0,0)/a_o$ as compared with an experimental value (14) of $2\pi(0.75,0,0)/a_o$. The width of the valence band as calculated is 21.1 ev which is in excellent agreement with the experimental result of 21 ev reported by Gora et al. (15), but is in substantial disagreement with the result 24.2 ev reported by McFeely et al. (16).

In general the band structure calculated from the initial iterative phase of this investigation is in excellent to good agreement with most available experimental measurements. The wavefunctions and band energies obtained from solution of the secular equation constructed with the self-consistent crystal potential represent solutions of Hartree-Fock-Slater problem for diamond. As mentioned in Chapter I, direct comparison of band structure with experiment can only be done reliably for a few measureable quantities. Also, examination of band structure reveals little about the more sensitive wavefunctions. A better test of a calculation then is to use the wavefunction solutions

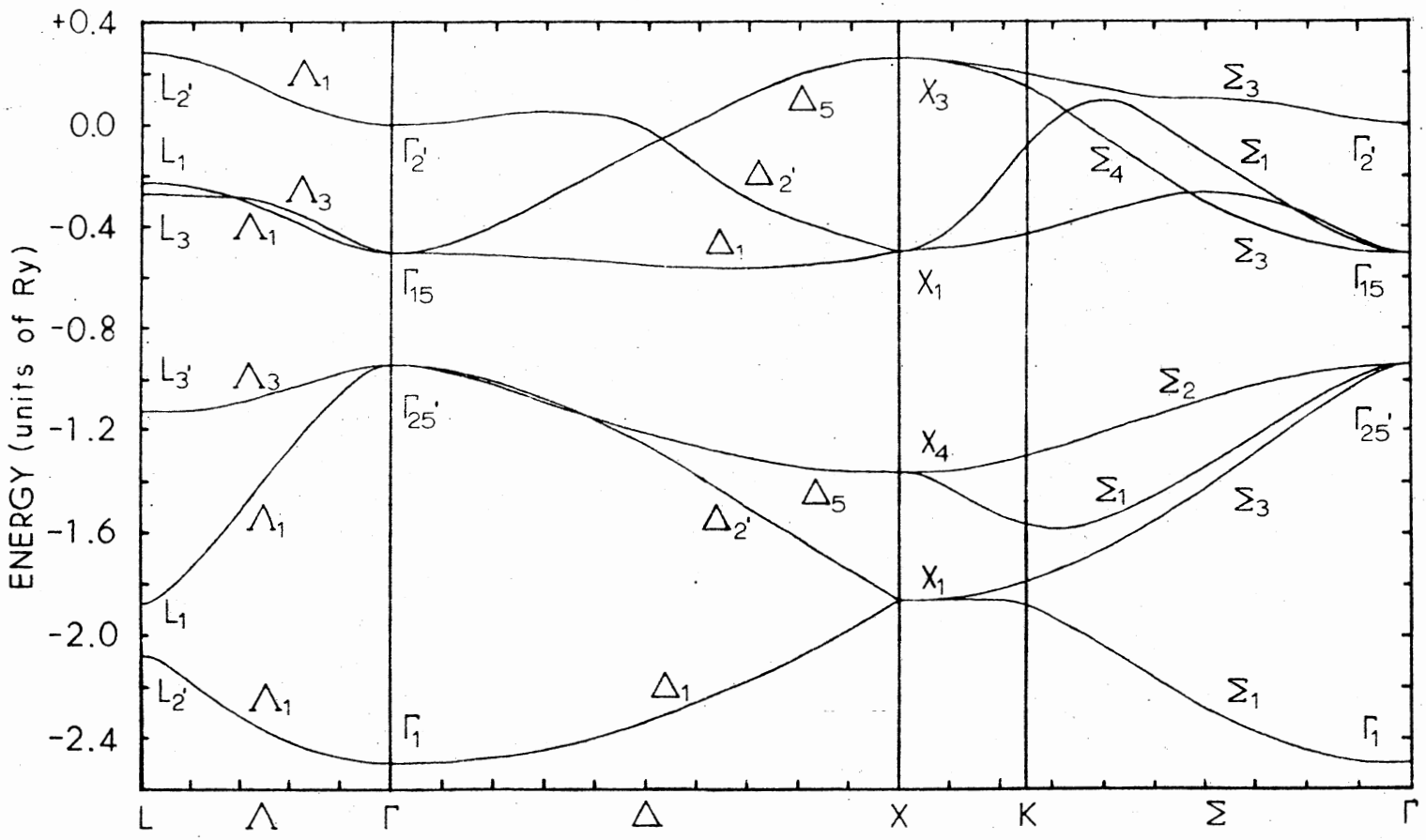

Figure 2. Self-consistent Band Structure of Diamond Using Optimized Orbital Basis

to the Hartree-Fock-Slater problem to evaluate bulk properties which can be measured experimentally, such as x-ray structure factors and Compton profile. With this objective, the remainder of this investigation will deal with the calculation of charge density and Compton profile.

CHAPTER III

BULK PROPERTIES

A. Charge Density and X-Ray Structure Factors

The absolute value of electronic charge density $\rho(\vec{r})$ for the λth iteration can be obtained directly from the wavefunctions $\psi^{\lambda}_{n,i}(\vec{k},\vec{r})$ by performing an integration over the Brillouin zone of the form

$$\rho^{\lambda}(\vec{r}) = \frac{2\eta}{\Omega_k} \int_{\Omega_k} \sum_{n,j} \psi^{\lambda *}_{n,j}(\vec{k},\vec{r})\, \psi^{\lambda}_{n,j}(\vec{k},\vec{r})\, d^3k, \tag{3.1}$$

where the sum over the indices n,j are over all occupied states at the point $\vec{k}$. Unfortunately, this integration can only be carried out numerically. The numerical integration scheme employed for this calculation is explained in detail in Appendix C. In order to evaluate this integral the integrand is first tabulated over a uniform mesh given by

$$\vec{K}_m = \frac{m_1 + \frac{1}{2}}{N_1} \cdot \frac{\vec{b}_1}{2} + \frac{m_2 + \frac{1}{2}}{N_2} \cdot \frac{3\vec{b}_2}{8} + \frac{m_3 + \frac{1}{2}}{N_3} \cdot \frac{\vec{b}_3}{2} \tag{3.2}$$

where $\vec{b}_1/2$, $3\vec{b}_2/8$ and $\vec{b}_3/2$ correspond to the edges of the irreducible wedge. Equation 3.1 is then replaced by the approximate expression

$$\rho^{\lambda}(\vec{r}) = \frac{4\eta}{\Omega_k} \sum_m \Delta_{k_m} \sum_{\gamma=1}^{24} \sum_{n,j} \psi^{\lambda *}_{n,j}(R_\gamma \vec{K}_m, \vec{r})\, \psi^{\lambda}_{n,j}(R_\gamma \vec{K}_m, \vec{r}), \tag{3.3}$$

where Δ_{k_m} is the volume of the fundamental wedge associated with $\vec{K}_m$ with

the restriction

$$\sum_m \Delta_{k_m} = \Omega_k/48$$

and R_γ is an element of the T_d site group symmetry. The wavefunctions $\psi_{n,j}(R_\gamma \vec{k}_m, \vec{r})$ are generated from $\psi_{n,j}(\vec{k}_m, \vec{r})$ by utilizing the unitary transformation given in Appendix A.

The expression given in Eq. 3.3 can be used to obtain the absolute value of electronic charge density $\rho^\lambda(\vec{r})$ for any point $\vec{r}$ of interest. The iterative process, as mentioned previously, will deal directly with $\rho(\vec{K}_\nu)$ and $\rho^{1/3}(\vec{K}_\nu)$. What is needed then is an analytic expression for $\rho^\lambda(\vec{r})$ of the form

$$\rho^\lambda_{f,t}(\vec{r}) = \sum_\nu \sum_i f_i^\lambda(\vec{r}-\vec{T}_{\nu i}) \quad . \tag{3.4}$$

This equation is very similar to Eq. 2.31 which was used in generating the starting potential. However, the functions will not be restricted to spherical symmetry alone. The fact that experiment gives a non-zero value for the "forbidden" reflection $\hat{k} = 2\pi(2,2,2)a_o$ indicates that higher order spherical harmonics are necessary to adequately represent the distortions of the crystal charge density due to the crystalline environment. Additionally, experiments done on crystal samples report different values for the x-ray structure factors associated with different stars with the same magnitude, which is another indication of non-spherical symmetry. These points are discussed in detail by Dawson (17). An analysis of the results of inclusion of higher order harmonics in $f_i^\lambda(\vec{r})$, in direct space, indicates this additional symmetry is used primarily in the critical bonding region. An example of this analysis,

in reciprocal space, is shown in Table I. In a self-consistent calculation where wavefunctions are allowed to relax to the crystalline environment through successive iterations this additional flexability might be crucial. In a recent self-consistent Hartree-Fock calculation for diamond and silicon by Hall (26), the spherical approximation was made and the resulting self-consistent x-ray from factors for the $\vec{K}_\sigma = 2\pi(1,1,1)/a_o$ reflection were in both cases substantially different from experiment. The x-ray form factor for this reflection is very sensitive to the bonding region and any incorrect representation of this region by relaxed self-consistent wavefunctions would be evident here. As a result of these considerations, the analytic form chosen for $f_i^\lambda(\vec{r})$ is a multipole expansion centered on an atom site in the first sublattice, which is expressed formally as

$$f_1^\lambda(\vec{r}) = \sum_\ell g_\ell^\lambda(r) \sum_m C_\ell^m Y_\ell^m(\hat{r}) \quad . \tag{3.5}$$

The summation over m is truncated after $\ell=4$. The tetrahedral site symmetry excludes $\ell=1$ and $\ell=2$ terms and allows for only one combination for each of the remaining terms: $\ell=0$, $\ell=3$ and $\ell=4$ referred to as monopole, octopole and hexadecapole, respectively. Because of inversion symmetry for diamond, the following restriction between the functions $f_1^\lambda(\vec{r})$ centered on atoms in sublattice one and $f_2^\lambda(\vec{r})$ for atoms on sublattice two is made, $f_1^\lambda(\vec{r}) = f_2^\lambda(-\vec{r})$. The final form of the fitting functions is given by

$$f_1^\lambda(\vec{r}) = g_o^\lambda(r) + g_3^\lambda(r)\left(\frac{xyz}{r^2}\right) + g_4^\lambda(r)(x^4 + y^4 + z^4 - 3r^4/5)/r^3. \tag{3.6}$$

After careful consideration of alternative forms, the $g_\ell^\lambda(r)$ were chosen

TABLE I

SELF-CONSISTENT HARTREE-FOCK-SLATER FOURIER COEFFICIENTS OF CHARGE DENSITY FOR DIAMOND, A COMPARISON OF VARIOUS COMPUTATIONAL TECHNIQUES

h ℓ ℓ	$\frac{\Omega}{2}\rho_o$	$\frac{\Omega}{2}\rho_{o,3}$	$\frac{\Omega}{2}\rho_{o,3,4}$	$\frac{\Omega}{2}[\rho]_6^{\dagger}$	$\frac{\Omega}{2}[\rho]_{19}$
111	-2.357	-2.356	-2.356	-2.356	-2.368
220	-2.013	-2.018	-2.017	-2.017	-2.022
311	-1.231	-1.234	-1.235	-1.235	-1.236
222	0.0	0.071	0.072	0.071	0.075
400	-1.621	-1.590	-1.589	-1.589	-1.590
331	1.101	1.105	1.105	1.104	1.106
422	1.457	1.451	1.452	1.452	1.452
511	0.993	0.994	0.991	0.991	0.991
333	0.993	0.988	0.986	0.986	0.986

†Where $[\rho]_6$ and $[\rho]_{19}$ correspond to 6-point and 19-point integrations, respectively, over the irreducible wedge.

to be

$$g_{\ell}^{\lambda}(r) = \sum_{i=1}^{8} \sigma_{\ell,i}^{\lambda} r^{n_i} e^{-N_i r} + \delta_{\ell,o} \sum_{i=9}^{12} \sigma_{o,i}^{\lambda} r^{n_i} e^{-N_i r}, \qquad (3.7)$$

where $\delta_{\ell,o} = \begin{cases} o \text{ for } \ell \neq o \\ 1 \text{ for } \ell = o \end{cases}$ and where the sets $\{n_i\}$ and $\{N_i\}$ are $\{0,1,2,3,4,5,6,7,0,0,0,0\}$ and $\{3,3,3,3,3,3,3,3,10,20,35,100\}$, respectively. The linear coefficients $\sigma_{\ell,i}^{\lambda}$ are determined by a least-squares fit to tabulated values of $\rho^{\lambda}(\vec{r})$. Because of the symmetric form of the fitting functions, $\rho^{\lambda}(\vec{r})$ is tabulated only on a uniform mesh over the irreducible volume. An additional mesh along two lines from the atom site at $\vec{t}_1$, is used to insure a good fit of the core charge density. All together charge density is tabulated at 256 points per iteration and an excellent analytic representation $\rho_{fit}^{\lambda}(\vec{r})$ of the electronic charge density throughout the crystal is obtained by performing a linear least squares fit to $\rho^{\lambda}(\vec{r})$ evaluated at these 256 points. Having found an analytic expression for charge density in terms of $\rho_{fit}^{\lambda}(\vec{r})$ this function can now be inserted into Eq. 2.13 and the Fourier coefficients $\rho^{\lambda}(\vec{K}_{\nu})$ determined. The details of performing the indicated integration in Eq. 2.13 for a multipole representation of charge density is given in Appendix D. In order to evaluate the adequacy of the fit and convergence of the multipole expansion, the self-consistent Fourier coefficients $\rho^{\lambda}(\vec{K}_{\nu})$ obtained using only the ℓ=o term, $\rho_{o}^{\lambda}(\vec{K}_{\nu})$ both the ℓ=o and ℓ=3 terms, $\rho_{o,3}^{\lambda}(\vec{K}_{\nu})$ and the ℓ=o, ℓ=3 and ℓ=4 terms, $\rho_{o,3,4}^{\lambda}(\vec{K}_{\mu})$ are presented in the second, third and fourth columns of Table I. In this calculation, the tabulated values of $\rho^{\lambda}(\vec{r})$ are obtained from Eq. 3.3 using a six-point numerical integration over the irreducible wedge. Examination of the columns in Table I established the validity of

truncating the multipole expansion at hexadecapole terms. It will also be shown in the next section that the quality of the fit obtained using the multipole expansion and radial fitting functions of the form $r^{n_i} e^{-\mu_i r}$ is exceptionally good.

In order to calculate $\rho^{1/3}(\vec{K}_\mu)$ a similar fitting procedure was employed. The multipole expansion representing $\rho^{1/3}(\vec{r})$ was determined from a linear least squares fit to the positive cube root of charge density tabulated over the same mesh in the irreducible volume. The functional form of the multipole expansion was the same with the exception of the set $\{\mu_i\}$ which was changed to {3,3,3,3,3,3,3,3,10,20,35, 50}.

An excellent fit was obtained with this choice for the fitting expansion. The multipole representation for $\rho^{1/3}(\vec{r})$ was substituted into an equation similar to Eq. 2.13 and the Fourier coefficients $\rho^{1/3}(\vec{K}_\mu)$ needed to construct the exchange potential were obtained.

One of the objectives of this investigation as set forth in the first chapter was the calculation of accurate x-ray structure factors. The multipole expansion procedure appears to satisfy this demand. However, it was decided an alternative procedure for evaluating $\rho^{\lambda}(\vec{r})$ was needed to test the quality of the fit and the validity of six-point integration over the fundamental wedge. In order to be a good test, this new procedure should be capable of more accuracy than the previous method and economical enough to be carried out using a larger number of integration points. The method that was developed satisfies all the above considerations. Using the notation of Eq. 2.37 for the wavefunctions $\psi^{\lambda}_{n,i}(\vec{k},\vec{r})$ and the symmetry property expressed in Eq. 2.24, it is shown in Appendix E that the Fourier components of charge density,

$\rho^{\lambda}(\vec{K}_{\mu})$ can be expressed

$$\rho^{\lambda}(\vec{K}_{\mu}) = \frac{2}{\Omega} \sum_{n} \sum_{\gamma} \int_{IW} Z^{\lambda}_{n,\gamma}(\vec{k},\vec{K}_{\mu}) d^3k, \tag{3.8}$$

where n is summed over all the occupied bands at point $\vec{k}$, the summation on γ is over all 48 operations R_{γ} of the cubic point group O_h and the integration is over the irreducible wedge. The integrand $Z^{\lambda}_{n,\gamma}(\vec{k},\vec{K}_{\mu})$ is given by

$$Z^{\lambda}_{n,\gamma}(\vec{k},\vec{K}_{\mu}) = \sum_{\nu} \sum_{j} e^{i(R_{\gamma}\vec{K}_{\mu})\cdot\vec{\tau}_{\gamma}} \xi^{\lambda *}_{n,j}(\vec{k},\vec{k} - R_{\gamma}(\vec{K}_{\nu} + \vec{K}_{\mu}))$$

$$\times \xi^{\lambda}_{n,j}(\vec{k},\vec{k} - R_{\gamma}\vec{K}_{\nu}) , \tag{3.9}$$

where the $\xi^{\lambda}_{n,j}(\vec{k},\vec{K})$ are related to $\xi^{\lambda}_{n,j}(\vec{k},\vec{r})$ by

$$\xi^{\lambda}_{n,j}(\vec{k},\vec{K}) = (2\pi)^{-\frac{3}{2}} \int \xi^{\lambda}_{n,j}(\vec{k},\vec{r})\, e^{-i\vec{K}\cdot\vec{r}}\, d\tau_r, \tag{3.10}$$

and where $\vec{\tau}_{\gamma}$ is the non-primitive translation associated with R_{γ}. The integration is again done numerically over the irreducible wedge using the uniform mesh given by Eq. 3.2. The self-consistent $\rho(\vec{K}_{\mu})$ which result from a six-point $[\rho(\vec{K}_{\mu})]_6$ and a nineteen-point $[\rho(\vec{K}_{\mu})]$ integration over the irreducible wedge are given in the last two columns of Table I. Comparison of $[\rho(K_{\mu})]_6$ with multipole expansion results demonstrates that the multipole expansion is well converged at the hexadecapole terms. An examination of the six-point and nineteen-point results reveals that they compare well for all $\rho(\vec{K}_{\mu})$ and the agreement improves with increasing $\vec{K}_{\mu}$. This trend is easily understood since the contribution to $\rho(\vec{K}_{\mu})$ from the core states becomes a rapidly dominant effect

with the increasing magnitude of $\vec{K}_\mu$. The core bands are flat with respect to the Brillouin zone and produce an integrand in Eq. 3.8 which is insensitive to the number of quadrature points. It is also clear from comparison of the last two columns of Table I that the nineteen-point numerical integration over the irreducible wedge is well converged with respect to the number of quadrature points. Even though the errors introduced by the six-point quadrature are minor even for small $\vec{K}_\mu$, the possibility of a cumulative effect resulting from the iterative procedure is eliminated by calculating the first nine $\rho(\vec{K}_\mu)$ for each iteration directly from Eq. 3.8 using the nineteen-point quadrature. The remaining $\rho(\vec{K}_\mu)$ are calculated using the multipole expansion and the six-point integration over the irreducible wedge.

The self-consistent Hartree-Fock-Slater x-ray structure factors $F^{SCF}_{HFS}(\vec{K}_\mu)$ for the limit of a rigid lattice are presented in the second column of Table II and are calculated from the Fourier coefficients of the self-consistent charge density presented in the last column of Table I using the relation

$$F^{SCF}_{HFS}(\vec{K}_\mu) = 4\Omega\rho(\vec{K}_\mu) \quad . \tag{3.11}$$

The self-consistent Hartree-Fock structure factors $F^{SCF}_{HF}(\vec{K}_\mu)$ of Euwema (18) are given in column three for comparison. The experimental structure factors of Göttlicher and Wöfel (19), corrected for the effects of isotropic thermal vibration, are given in column four. The agreement between the theoretical results of column two and the experimental results of column four is good for all reflections, except the 400 reflection, which is in significant disagreement. It is interesting to note that the largest disagreement between experiment and the Hartree-Fock

TABLE II

X-RAY STRUCTURE FACTORS FOR DIAMOND

h k ℓ	F^{SCF}_{HFS}	F^{SCF}_{HF} (a)	F_{EXP} (b)
111	-18.945	-18.657	-18.787
220	-16.181	-15.445	-15.778
311	- 9.886	- 9.456	- 9.405
222	0.601	0.689	1.206(c)
400	-12.718	-12.359	-11.836
331	8.847	8.637	8.932
422	11.615	11.339	11.547
511	7.926		8.023
333	7.884		8.023

(a) Ref. (8).

(b) Ref. (18).

(c) Weiss and Middleton in private communication to B. Dawson (Ref. 19).

results of Euwema is again the 400 reflection. With the exception of this reflection, the two theoretical results stand in substantially equivalent agreement with experiment. A useful gauge for comparison between experiment and theory is the agreement factor given by

$$R = \Sigma|F_{EXP} - F_{THEORY}|/\Sigma|F_{EXP}| \quad . \tag{3.12}$$

The agreement factors for Hartree-Fock-Slater and Hartree-Fock are 3.4% and 2.7%, respectively.

A further examination of Table II indicates the Hartree-Fock-Slater form factors are generally larger than experiment. This is consistent with the conclusions of Dawson (25) that the experimental results of Göttlicher and Wöfel must be multiplied by a scale factor of 1.007 in order to renormalize to absolute intensity. In the present investigation the scale factor which minimizes the agreement factor between the Hartree-Fock-Slater form factors and those of experiment is 1.008, which is in excellent agreement with Dawson.

B. Compton Profile

Another bulk property which can be calculated from the self-consistent wavefunctions and compared to experiment is Compton profile. A method for calculating the theoretical Compton profiles using the impulse approximation (20) has been developed and is presented in Appendix F. Within the impulse approximation, the Compton profile $J(q,\hat{k})$ is related to the self-consistent wavefunctions by the expression

$$J(q,\hat{k}) = \int \delta(q-\hat{k}\cdot\vec{K})\ \rho(\vec{K})\ d^3K \quad , \tag{3.13}$$

where $\rho(\vec{K})$ is the momentum density per atom given by

$$\rho(\vec{K}) = \Omega_k^{-1} \int_{\Omega k} \sum_n \sum_j \psi^*_{n,j}(\vec{k},\vec{K})\ \psi_{n,j}(\vec{k},\vec{K})\ d^3k\ , \qquad (3.14)$$

and where the summations on n and j are over the six occupied band states of each point $\vec{k}$ in the Brillouin zone. The $\psi_{n,j}(\hat{k},\vec{K})$ of Eq. 3.14 are the band states in momentum representation and given by

$$\psi_{n,j}(\vec{k},\vec{K}) = (2\pi)^{-3/2} \int \psi_{n,j}(\vec{k},\vec{r})\ e^{-i\vec{K}\cdot\vec{r}}\ d\tau_r\ . \qquad (3.15)$$

If the wavefunctions are written in the form of Eq. 2.37, then utilization of the translational symmetry of the Bloch sum reduces the momentum density $\rho(\vec{K})$ given in Eq. 3.14 to the simple analytic expression

$$\rho(\vec{K}) = \sum_n \sum_j \left|\xi_{n,j}(\vec{K},\vec{K})\right|^2\ , \qquad (3.16)$$

where $\xi_{n,j}(\vec{K},\vec{K})$ are given by Eq. 3.10 and are periodic in $\vec{K}$-space with respect to the first index so that

$$\left|\xi_{n,j}(\vec{K}+\vec{K}_\mu,\vec{K})\right|^2 = \left|\xi_{n,j}(\vec{K},\vec{K})\right|^2\ .$$

The integral over reciprocal space in Eq. 3.13 is re-expressed as a sum of integrals over the Brillouin zone resulting in

$$J(q,\hat{k}) = \sum_\mu \int_{\Omega_k} \delta(q-\hat{k}\cdot(\vec{k}+\vec{K}_\mu))\ \rho(\vec{k}+\vec{K}_\mu)\ d^3k\ . \qquad (3.17)$$

A useful symmetry relation involving the momentum density can be derived using Eq. 3.14 and the transformation properties of Eq. 2.29, it is

$$\rho(R_\gamma\vec{K}) = \rho(\vec{K}) \qquad (3.18)$$

for all operations R_γ of the point group O_h. By using this symmetry relation and Eq. 3.17 the Compton profile can be reduced to a sum of integrations over the irreducible wedge of the form

$$J(q,\hat{k}) = \sum_\mu \sum_\gamma \int_{IW} \delta(q-(R_\gamma \hat{k})\cdot(\vec{k}+\vec{K}_\mu)) \; \rho(\vec{k}+\vec{K}_\mu) \; d^3k \qquad (3.19)$$

As expressed in this equation, the Compton profile is obtained from a series of integrations over a family of planes which intersect some portion of the irreducible wedge.

A numerical procedure for calculating $J(q,\hat{k})$ is obtained by rewriting Eq. 3.19 as

$$J(q,\hat{k}) = \sum_\mu \sum_\gamma \bar{\rho}_\mu(q-(R_\gamma \hat{k})\cdot\vec{K}_\mu, R_\gamma \hat{k}) \; x \; A(q-(R_\gamma \hat{k})\cdot\vec{K}_\mu, R_\gamma \hat{k}) \; , \qquad (3.20)$$

where $A(\lambda,\hat{n})$ is the area of the segment of the plane $\vec{K}\cdot\hat{n} = \lambda$ which lies within the irreducible wedge and λ is the distance to the origin along the $\hat{n}$ direction: i.e.,

$$A(\lambda,\hat{n}) = \int_{IW} \delta(\lambda-\vec{k}\cdot\hat{n}) \; d^3k \qquad (3.21)$$

and for this case $\hat{n}$ and λ are given by

$$\hat{n} = R_\gamma \hat{k}$$

and

$$\lambda = q-(R_\gamma \hat{k})\cdot\vec{K}_\mu = (R_\gamma \hat{k})\cdot\vec{k} \; .$$

The term $\bar{\rho}_\mu(\lambda,\hat{n})$ is the average of $\rho(\vec{k}+\vec{K}_\mu)$ over this same area segment. In calculating the Compton profile for diamond, the areas of the planes

intersecting the irreducible wedge $A(\lambda,\hat{n})$ are evaluated analytically and the averages $\bar{\rho}_\mu(\lambda,\hat{n})$ are evaluated numerically by first tabulating $\rho(\vec{k}+\vec{K}_\mu)$ over the uniform mesh

$$\vec{k}'_m = |n_1\vec{b}_1 + n_2\vec{b}_2 + n_3\vec{b}_3)/N \ , \qquad (3.22)$$

where n_1, n_2, n_3 are integers so chosen that $\vec{k}'_m$ lies within or upon the surface of the irreducible wedge and N controls the density of points. The numerical integration for $J(q,\hat{k})$ was done for the five different $\hat{k}$ directions using different values for N. It was found that the first three symmetry directions (1,0,0), (1,1,0) and (1,1,1) were sufficiently converged with a value of ten for N. However, two remaining directions (2,1,1) and (2,2,1) were noisy for this choice of N due to the low density of points per plane. The final calculations were performed using an N value of 20 for which all five directions were well converged with respect to the numerical integration.

The self-consistent Hartree-Fock-Slater Compton profile for $\hat{k}$ = (1,0,0) is presented in Figure 3 by the solid line. Evenly spaced data points are indicated by solid dots. The experimental measurements of Weiss and Phillips (21) are plotted for comparison with open circles. The theoretical predictions of the self-consistent Hartree-Fock calculation by Wepfer, Euwema, Surratt and Wilhite (23) are also plotted and indicated by triangles. The other four directions with a similar comparison of theoretical and experimental results are shown in Figure 4. The comparison between the Hartree-Fock-Slater predictions of the present work and experiment is very good for all five directions. Agreement is generally better in the second half of the Compton profile where the core states start to have a major contribution. A similar

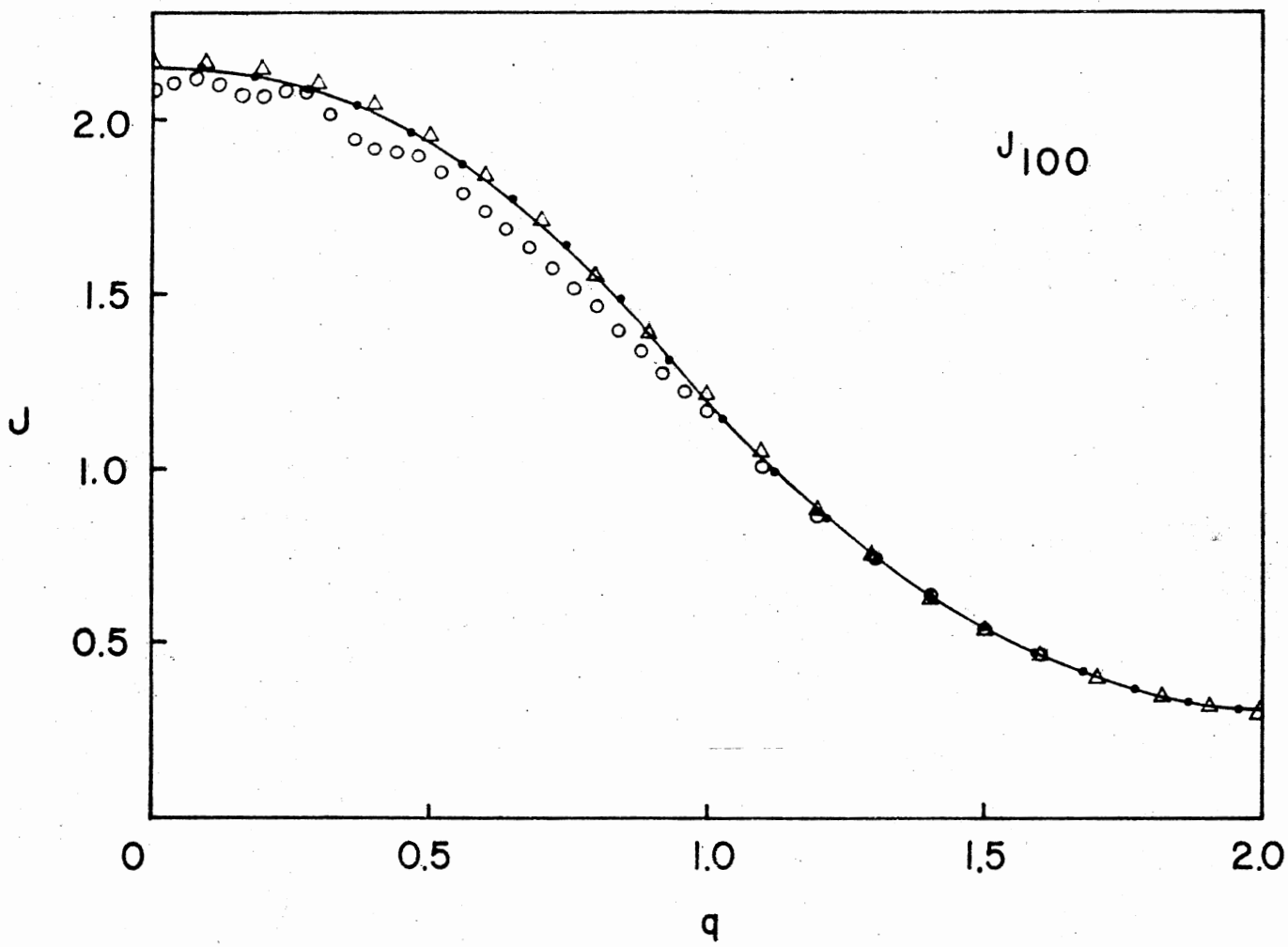

Figure 3. Compton Profile $J(q,\hat{k})$ for $\hat{k} = (1,0,0)$. The open circles are the experimental results of Weiss and Phillips (Ref. 21), the triangles are the self-consistent Hartree-Fock calculations of Wepfer, et al. (Ref. 23), and the dots connected by the solid curve are the self-consistent Hartree-Fock-Slater results of the present work. Values of q and J are given in atomic units

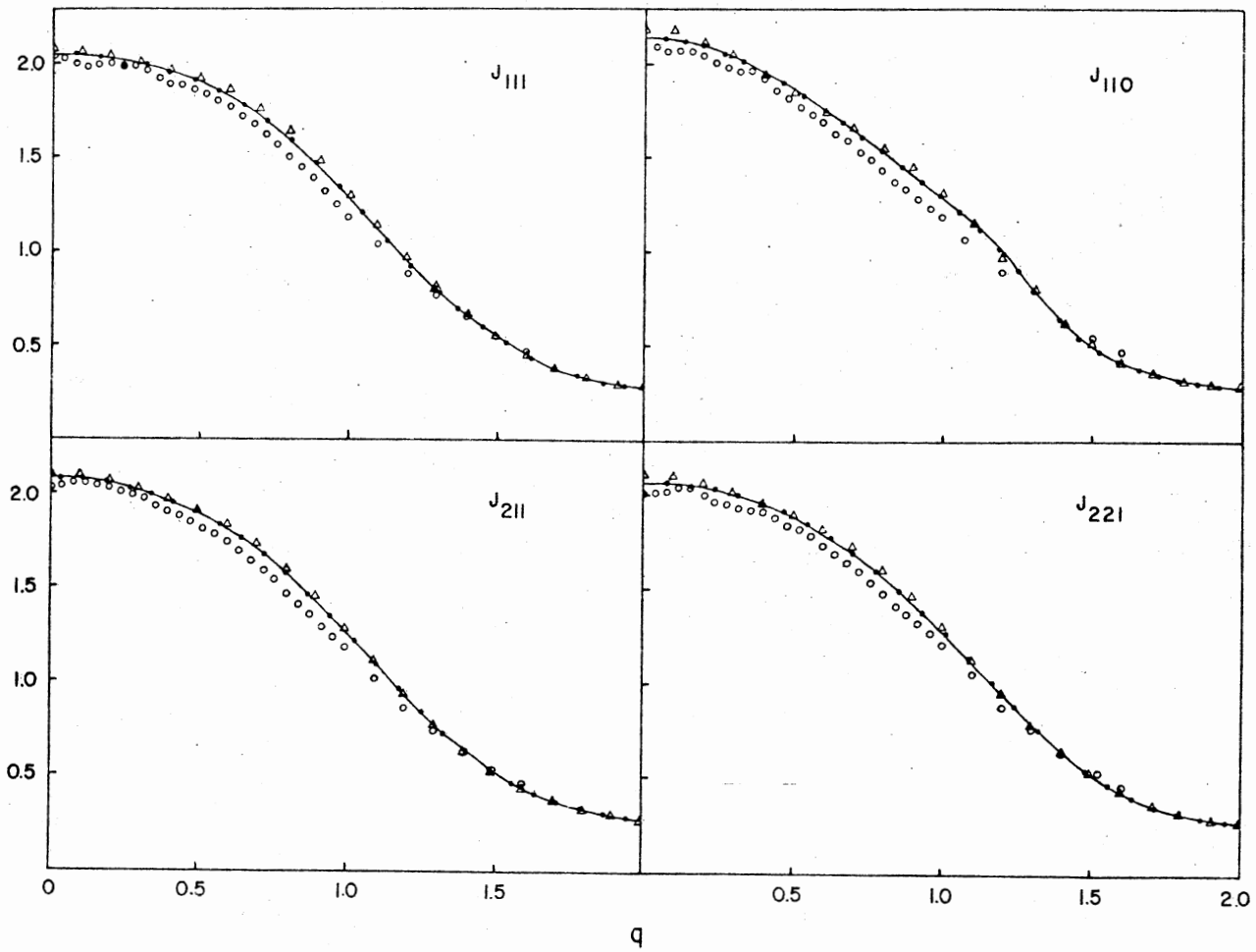

Figure 4. Compton Profiles for Lower Symmetry Directions. The open circles are the experimental results of Weiss and Phillips (Ref. 21), the triangles are the self-consistent Hartree-Fock calculations of Wepfer, et al. (Ref. 23) and the dots connected by the solid curve are the self-consistent Hartree-Fock-Slater results of the present work. Values of q and J are given in atomic units

comparison between the predictions of the present work and Hartree-Fock reveals surprisingly excellent agreement. For all the directions presented, the two theoretical calculations agree with each other even better than with experiment.

A more illuminating comparison of theory and experiment is obtained by examining the anisotropies in the Compton profiles associated with different scattering directions. The anisotropies have been measured directly by Reed and Eisenberger (22) who referenced their experiment results to the scattering direction (1,0,0). These experimental results are reproduced approximately in Figure 5 by open circles connected by straight lines. The self-consistent Hartree-Fock-Slater results are given in Figure 5 by the filled circles and the self-consistent Hartree-Fock results are presented by triangles. Considering that the anisotropies are more than an order of magnitude smaller than the total Compton profile, the agreement between the present work and the experimental results is exceptionally good. Again, the agreement between Hartree-Fock-Slater and Hartree-Fock is quite remarkable. In fact for three of the anisotropies the two theoretical results are virtually identical for the second half of the anisotropy.

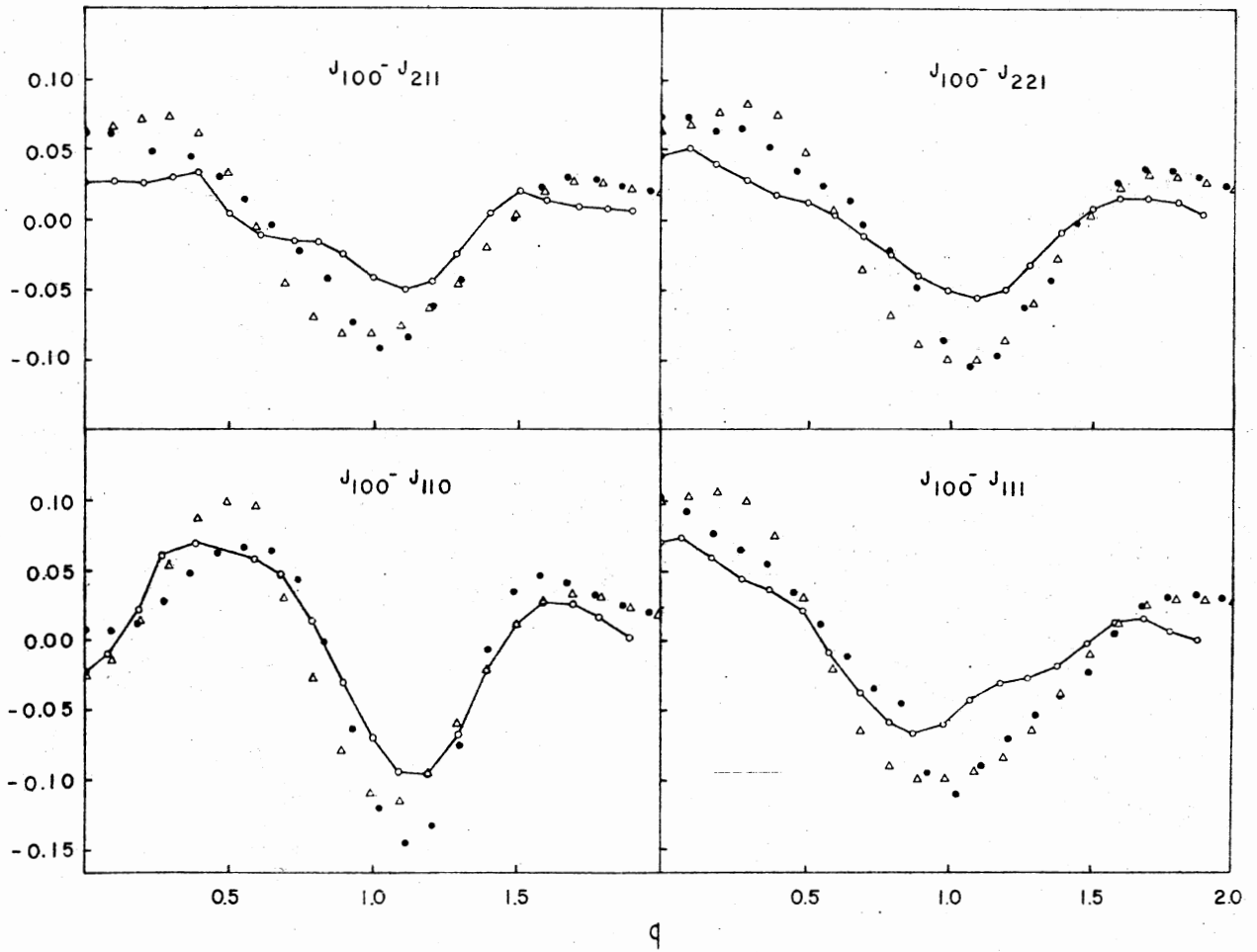

Figure 5. Anisotropy of Compton Profile. The open circles connected by solid lines are the experimental results of Reed and Eisenberger (Ref. 22), the triangles are the self-consistent Hartree-Fock calculations of Wepfer, et al. (Ref. 23), and the solid circles are the self-consistent Hartree-Fock-Slater calculations of the present work. Values of q and J are given in atomic units

CHAPTER IV

SUMMARY AND CONCLUSIONS

In this investigation a procedure for doing a self-consistent Hartree-Fock-Slater calculation and obtaining accurate wavefunctions and band energies was presented. The use of optimized orbitals provided the flexability of utilizing a large amount of variational freedom while maintaining a small basis set. The optimized orbitals were chosen to be representative of the valance band and were re-optimized with each successive iteration to allow for relaxation to the crystalline environment. The new crystal potential for each iteration was generated directly from the previous iteration charge density. Two methods were used to calculate the charge density in order to test the accuracy of the evaluation. The first method utilized a multipole expansion which was obtained from a six-point integration over the irreducible wedge of the Brillouin zone and was found to be well converged at the hexadecapole terms. The resulting Fourier coefficients of charge density were found to be accurate with the exception of the longest wavelength coefficients for which a nineteen-point quadrature was necessary. The second method is a procedure of obtaining the Fourier coefficients of charge density directly from the wavef-nctions. It is an original and highly useful technique of evaluating the Fourier coefficients of charge density and was used to insure the accuracy of the more sensitive long wavelength coefficients.

coefficients.

The self-consistent Hartree-Fock-Slater band structure predicts an indirect band gap which is in good agreement with experiment as to magnitude and location of the minimum in the conduction band. The x-ray structure factors evaluated from self-consistent wavefunctions agree reasonably well with the experimental results of Göttlicher and Wöfel. However, a careful analysis reveals trends which tend to support the conclusion of Dawson's exhaustive studies on diamond that the measurements of Göttlicher and Wöfel are not normalized to absolute intensity and need to be multiplied by a scale factor of 1.007. In light of some of the advances in experimental technique which have been made since this experiment was originally done, a re-evaluation of the experimental x-ray structure factors for diamond would seem in order. As an additional test of the self-consistent wavefunctions, theoretical Compton profiles were calculated and compared to experimetal measurements. In all directions examined, agreement between theory and experiment was excellent. A sensitive test of Compton profile is obtained by analyzing the anisotrophies. The agreement between the theoretical and experimental anisotropies was also found to be excellent.

A comparison between the predictions of the present work and a self-consistent Hartree-Fock calculation for both x-ray structure factors and Compton profile was made. Diamond is one of the few crystals for which a self-consistent Hartree-Fock calculation has been done and very few direct comparisons of the two methods have ever been made. The results of this comparison showed that Hartree-Fock-Slater was in slightly better agreement with experiment for Compton profile and the situation was reversed for x-ray structure factors. Also, one of the

more surprising results is the remarkable agreement between the Compton profiles predicted by these two theories. In general, it appears that despite the considerable conceptual differences between these two theories, they predict bulk properties which are in substantially similar agreement with experiment when carried to self-consistency. This is true despite the real differences between the band structures predicted by the two theories.

REFERENCES

1. Herring, C., Phys. Rev. 57, 1169 (1949).

2. Korring, J., Physica 13, 392 (1947); Kohn, W. and N. Rostoker, Phys. Rev. 94, 1111 (1954).

3. Bloch, F., Z. Physik 52, 555 (1928).

4. Lafon, E. E. and C. C. Lin, Phys. Rev. 152, 579 (1966).

5. Chaney, R. C., T. K. Tung, C. C. Lin, and E. E. Lafon, J. Chem. Phys. 52, 361 (1970).

6. Kervin, P. W. and E. E. Lafon, Phys. Rev. 58, 1535 (1973).

7. Wang, C. S. and J. Callaway, Phys. Rev. B 11, 2417 (1975).

8. Ching, W. Y. and C. C. Lin, Phys. Rev. B 14, 620 (1976).

9. Slater, J. C., Quantum Theory of Atomic Structure, Vol. 2, McGraw-Hill, New York (1960).

10. Huizinga, S., J. Chem. Phys. 42, 1293 (1965).

11. Chaney, R. C., E. E. Lafon and C. C. Lin, Phys. Rev. B 3, 459 (1971).

12. Chaney, R. C., E. E. Lafon, and C. C. Lin, Phys. Rev. B 4, 2734 (1971).

13. Clark, C. D., P. J. Dean and P. V. Harris, Proc. R. Soc. Lond. A 277, 312 (1964).

14. Dean, P. J., E. C. Lightowlers, and D. R. Wight, Phys. Rev. 140, A352 (1965).

15. Gora, T., R. Staley, J. D. Rimstidt, and J. Sharma, Phys. Rev. B 5, 2309 (1972).

16. McFeely, F. R., S. P. Kowalczyk, L. Ley, R. G. Lavell, R. A. Pollak, and D. A. Shirley, Phys. Rev. B 9, 5268 (1974).

17. Dawson, B., Proc. R. Soc. Lond., 298, 255 (1967).

18. Euwema, R. N., D. L. Wilhite, and G. T. Surratt, Phys. Rev. B 7, 818 (1973).

19. Göttlicher and E. Wöfel, Z. Elektrochem, 63, 891 (1959).

20. Eisenberger, P. and P. M. Platzman, Phys. Rev. A 2, 415 (1970).

21. Weiss, R. J. and W. C. Phillips, Phys. Rev. 176, 900 (1968).

22. Reed, W. A. and P. Eisenberger, Phys. Rev. B 6, 4596 (1972).

23. Wepfer, G. G., R. N. Euwema, G. T. Surratt, and D. L. Wilhite, Phys. Rev. B 9, 2670 (1974).

24. Simmons, J. E., C. C. Lin, D. F. Fouquet, E. E. Lafon, and R. C. Cheney, J. Phys. C 8, 1954 (1975).

25. Dawson, B., Proc. R. Soc. Lond. A 298, 264 (1967).

26. Hall, K., Ph.D. Dissertation (University of Illinois at Urbana-Champaign, 1976).

APPENDIX A

TRANSFORMATION OF MATRIX ELEMENTS AND EIGENVECTORS UNDER SYMMETRY OPERATIONS IN THE BRILLOUIN ZONE

If the origin is placed on sublattice one, then the Bloch sums can be written

$$b_i^{\Delta}(\vec{k},\vec{r}) = I_i^{\Delta}(b_i'^{1}(\vec{k},\vec{r}) + \Delta b_i'^{2}(\vec{k},\vec{r})) \tag{A-1}$$

where

$$b_i'^{1}(\vec{k},\vec{r}) = r^{-\frac{1}{2}} \sum_{\nu} e^{i\vec{k}\cdot\vec{R}_\nu} \psi_i(\vec{r}-\vec{R}_\nu), \tag{A-2}$$

$$b_i'^{2}(\vec{k},\vec{r}) = n^{-\frac{1}{2}} \sum_{\nu} e^{i\vec{k}\cdot\vec{R}_\nu} \phi_i(\vec{r}-(\vec{R}_\nu+\vec{t})), \tag{A-3}$$

and where

$$\Delta = \pm 1;\ \vec{t} = a_o(1,1,1)/4;\ i = s,p;$$

$$\ell_i = \begin{cases} 0 \text{ for } i = s \\ 1 \text{ for } i = p \end{cases}$$

$$I_i^{\Delta} = (i)^{\ell_i+\ell_\Delta},\ \ell_\Delta = \begin{cases} 0 \text{ for } \Delta = +1 \\ 1 \text{ for } \Delta = -1 \end{cases}.$$

It is straightforward to show that the Bloch sums on sublattice one and two transform according to

$$b_i'^{\delta}(R_\alpha\vec{k},R_\alpha\vec{r}+\vec{t}_\alpha) = \sum_{\delta'=1}^{2} \Omega_{i\alpha}^{\delta\delta'}(\vec{k}) \sum_j R_{ij}^{\alpha} b_j'^{\delta'}(\vec{k},\vec{r}), \tag{A-4}$$

where

$$\Omega_{i,\alpha}(\vec{k}) = \begin{pmatrix} 1 & 0 \\ 0 & e^{-i\theta} \end{pmatrix}, \text{ if } R_\alpha = \tau_\alpha \text{ and } \tau_\alpha \varepsilon T_d; \tag{A-5}$$

$$\Omega_{i,\alpha}(\vec{k}) = \begin{pmatrix} 0 & e^{-i\theta} \\ 1 & 0 \end{pmatrix}, \text{ if } R_\alpha = \tau_\alpha I \text{ and } \tau_\alpha \varepsilon T_d; \tag{A-6}$$

and

$$\theta = \tau_\alpha \vec{k} \cdot (\vec{t} - \tau_\alpha \vec{t}) \ . \tag{A-7}$$

Now define the matrix A_i by the relation

$$A_i = \begin{pmatrix} I_i^+ & I_i^+ \\ I_i^- & -I_i^- \end{pmatrix} = (i)^{\ell_i} \begin{pmatrix} 1 & 1 \\ i & -i \end{pmatrix} \tag{A-8}$$

and use it to rewrite Eq. A-1 as

$$b_i^\Delta(\vec{k},\vec{r}) = \sum_{\delta=1}^{2} A_i^{\Delta\delta} \, b_i'^{\delta}(\vec{k},\vec{r}) \tag{A-9}$$

and the reciprocal relationship is expressed

$$b_i'^{\delta}(\vec{k},\vec{r}) = \sum_{\Delta} (A_i^{-1})^{\delta\Delta} \, b_i^\Delta(\vec{k},\vec{r}) \ . \tag{A-10}$$

Therefore, using the result of Eq. A-4, the Bloch sums must transform according to the condition,

$$b_i^\Delta(R_\alpha \vec{k}, \ R_\alpha \vec{r} + \vec{t}_\alpha) = \sum_{j,\Delta'} \Lambda_{ij}^{\Delta\Delta'}(\alpha,\vec{k}) \, b_j^{\Delta'}(\vec{k},\vec{r}) \tag{A-11}$$

where

$$\Lambda_{ij}^{\Delta\Delta'}(\alpha,\vec{k}) = (\sum_{\delta,\delta'} A_i^{\Delta\delta}\, \Omega_{i\alpha}^{\delta\delta'}(\vec{k})(A_i^{-1})^{\delta'\Delta'})R_{ij}^{\alpha} \qquad \text{(A-12)}$$

substituting the expressions for A_i and $\Omega_{i\alpha}(\vec{k})$ into Eq. A-12 results in the equation

$$\Lambda_{ij}^{\Delta\Delta'}(\alpha,\vec{k}) = e^{-i\frac{\theta}{2}} \begin{pmatrix} \cos\frac{\theta}{2} & \sin\frac{\theta}{2} \\ -\sin\frac{\theta}{2} & \cos\frac{\theta}{2} \end{pmatrix}^{\Delta\Delta'} R_{ij}^{\alpha} \text{ if } R_\alpha = \tau_\alpha \qquad \text{(A-13)}$$

and

$$\Lambda_{ij}^{\Delta\Delta'}(\alpha,\vec{k}) = e^{-i\frac{\theta}{2}} \begin{pmatrix} \cos\frac{\theta}{2} & \sin\frac{\theta}{2} \\ \sin\frac{\theta}{2} & -\cos\frac{\theta}{2} \end{pmatrix}^{\Delta\Delta'} R_{ij}^{\alpha} \text{ if } R_\alpha = \tau_\alpha I \qquad \text{(A-14)}$$

for which $\tau_\alpha \in T_d$ and I is the inversion operator. Now let the operator θ stand for H or $\hat{1}$ then consider the following integral

$$O_{ii'}^{\Delta\Delta'}(\vec{k}) = \int b_i^{*\Delta}(\vec{k},\vec{r})\ \theta b_{i'}^{\Delta'}(\vec{k},\vec{r})d\tau_r \qquad \text{(A-15)}$$

and for the corresponding rotated point in the Brillouin zone

$$O_{ii'}^{\Delta\Delta'}(R_\alpha\vec{k}) = \int b_i^{*\Delta}(R_\alpha\vec{k},\vec{r})\ \theta b_i^{\Delta'}(R_\alpha\vec{k},\vec{r})d\tau_r, \qquad \text{(A-16)}$$

which is related to the unrotated matrix element by

$$O_{ii'}^{\Delta\Delta'}(R_\alpha\vec{k}) = \sum_{j,\bar{\Delta}} \sum_{j',\bar{\Delta}'} \Lambda_{ij}^{\Delta\bar{\Delta}*}(\alpha,\vec{k}) O_{jj'}^{\bar{\Delta}\bar{\Delta}'}(\vec{k}) \tilde{\Lambda}_{j'i'}^{\bar{\Delta}'\Delta'}(\alpha,\vec{k}) \qquad \text{(A-17)}$$

or in matrix notation

$$O(R_\alpha\vec{k}) = \Lambda^*(\alpha,\vec{k})\ O(\vec{k})\ \tilde{\Lambda}(\alpha,\vec{k})\ . \qquad \text{(A-18)}$$

Using this symmetry relation in conjunction with the secular equation

it is easy to show the Eigenvectors are related

$$C_n(R_\alpha \vec{k}) = U(\alpha,\vec{k})\, C_n(\vec{k}), \tag{A-19}$$

where

$$U(\alpha,\vec{k}) = e^{i\frac{\theta}{2}}\, \Lambda(\alpha,\vec{k}) \ . \tag{A-20}$$

APPENDIX B

THE IRREDUCIBLE VOLUME

The use of crystal symmetry is a great aid in reducing the number of redundant calculations. For example, the electronic charge density $\rho(\vec{r})$ for diamond evaluated at some point $\vec{r}$ must obey the condition

$$\rho(\vec{r}) = \rho(R_\gamma \vec{r} + \vec{\tau}_\gamma) \tag{B-1}$$

where R_γ is an element of T_d and $\vec{\tau}_\gamma$ is the corresponding non-primitive translation vector. Hence, charge density needs only to be evaluated over an irreducible volume within the Wigner-Seitz unit cell. The criterion of irreducibility is that the volume chosen must reproduce the entire Wigner-Seitz unit cell when operated on by all 48 operations. Obviously, the volume of the irreducible volume is $\Omega/48$. If the glide plane ($\vec{r} \rightarrow -\vec{r} + a_o(1,1,1)/4$) is neglected, the irreducible volume will have a volume $\Omega/24$ and one possible choice for this volume would be

$$x \geq y \geq |z| \geq 0 , \tag{B-2}$$

$$x + y \geq a_o/2 . \tag{B-3}$$

However, use of this volume would still result in redundant calculations. In order to reduce this volume further, the glide plane symmetry must be taken into account. When this is done the irreducible volume chosen in this investigation, consists of three wedges:

wedge one consists of the collection of points which obey the conditions

$$x, y, z \leq 0 \ , \tag{B-4}$$

$$|x| \geq |y| \geq |z| \ , \tag{B-5}$$

and

$$|x| \leq a_o/4 \ ; \tag{B-6}$$

wedge two contains points which obey the conditions

$$x, y, z > 0 \ , \tag{B-7}$$

$$x \geq y \geq z \ , \tag{B-8}$$

$$x < a_o/4 \tag{B-9}$$

and

$$\hat{n} \cdot \vec{r} \leq \sqrt{3} \ (a_o/8) \ , \tag{B-10}$$

where

$$\hat{n} = (1,1,1)/\sqrt{3}$$

and

$$\vec{r} = (x,y,z) \ ;$$

wedge three contains points which obey the conditions

$$x > a_o/4 \ , \tag{B-11}$$

$$x+y < a_o/z \ , \tag{B-12}$$

$$y+z > 0 \ , \tag{B-13}$$

$$z < 0 \tag{B-14}$$

and

$$x-y + z > a_o/8 \ . \tag{B-15}$$

APPENDIX C

INTEGRATION BY PARALLELEPIPED QUADRATURE

The numerical integration over the irreducible wedge used in evaluating charge density is a technique of partioning the volume of integration into equivalent parallelepipeds. The center points of the parallelepipeds are given by

$$\vec{k}_m = \frac{m_1 + \frac{1}{2}}{N_1} \cdot \frac{\vec{b}_1}{2} + \frac{m_2 + \frac{1}{2}}{N_2} \cdot \frac{3\vec{b}_2}{8} + \frac{m_3 + \frac{1}{2}}{N_3} \cdot \frac{\vec{b}_3}{2} \qquad \text{(C-1)}$$

where N_1, N_2 and N_3 are integers which control the density of points and are chosen so that

$$\left|\frac{\vec{b}_1}{N_1}\right| \approx \left|\frac{\vec{b}_2}{N_2}\right| \approx \left|\frac{\vec{b}_3}{N_3}\right|$$

The vectors $\vec{b}_{1/2}$, $3\vec{b}_{2/8}$, $\vec{b}_{3/2}$ correspond to the edges of the irreducible wedge. The integers m_1, m_2 and m_3 are chosen so that some of the volume of parallelepiped lies within the irreducible wedge. This results in the three conditions:

1. m_1, m_2 and $m_3 \geq 0$, (C-2)

This restricts the parallelepipeds from having any volume outside the side surfaces of the irreducible wedge;

2. $$\frac{4m_1}{N_1} + \frac{3m_2}{N_2} + \frac{2m_3}{N_3} < 4 \qquad \text{(C-3)}$$

and

$$3. \quad \frac{2m_1}{N_1} + \frac{3m_2}{N_2} + \frac{3m_3}{N_3} < 3 \ , \tag{C-4}$$

these conditions insure that at least part of the parallelepiped is inside the wedge. The volume of the parallelepiped, $\Delta\tau_k$, is given by

$$\Delta\tau_k = \left| \frac{3\vec{b}_1 \cdot (\vec{b}_2 x \vec{b}_3}{32\ N_1 N_2 N_3} \right| = \frac{3(\pi/a_o)^3}{N_1 N_2 N_3} \tag{C-5}$$

The integrand contained in each parallelepiped is weighted by the volume of the para-lelepiped which lies within the wedge. The sum of the weighting factors Δ_{k_m} must obey the restriction

$$\sum_n \Delta_{k_m} = \Omega_{k/48} \tag{C-6}$$

where $\Omega_{k/48}$ is the volume of irreducible wedge.

APPENDIX D

THE FOURIER TRANSFORM OF A MULTIPOLE EXPANSION OF CHARGE-DENSITY

The multipole expansion representation of the electronic portion of the crystal charge density as presented in Chapter III is given by

$$\rho^{\lambda}_{fit}(\vec{r}) = \sum_{\nu} \sum_{i} f^{\lambda}_{i}(\vec{r}-\vec{T}_{\nu i}), \tag{D-1}$$

where the functional form of $f^{\lambda}_{l}(\vec{r})$ is written as

$$f^{\lambda}_{l}(\vec{r}) = \sum_{\ell} g^{\lambda}_{\ell}(r) \sum_{m} C^{m}_{\ell} Y^{m}_{\ell}(\hat{r}). \tag{D-2}$$

The corresponding Fourier coefficients of charge density are expressed in terms of this representation as

$$\rho^{\lambda}(\vec{K}_{\mu}) = \frac{1}{n\Omega} \sum_{\nu} \sum_{i} \int_{n\Omega} f^{\lambda}_{i}(\vec{r}-\vec{T}_{\nu i}) e^{-i\vec{K}_{\mu}\cdot\vec{r}} \, d\tau_{r} \tag{D-3}$$

It is easy to show that by transforming the variable of integration while utilizing the translational and inversion symmetry the previous equation reduces to the expression

$$\rho^{\lambda}(\vec{K}_{\mu}) = \frac{1}{\Omega} \left[e^{-i\vec{K}_{\mu}\cdot\vec{t}_{l}} \int f^{\lambda}_{l}(\vec{r}) e^{-i\vec{K}_{\mu}\cdot\vec{r}} \, d\tau_{r} + e^{i\vec{K}_{\mu}\cdot\vec{\tau}_{l}} \int f^{\lambda}_{l}(-\vec{r}) e^{-i\vec{K}_{\mu}\cdot\vec{r}} \, d\tau_{r} \right] \tag{D-4}$$

A further evaluation of Eq. (D-4) will be aided by first examining an integral of the form

$$\chi(\ell,m,\vec{k},r) = \phi\, Y_{\ell m}(\theta,\phi)e^{-i\vec{k}\cdot\vec{r}}\, d\bar{\Omega} \qquad \text{(D-5)}$$

where the equation is integrated over the solid angle $\bar{\Omega}$. The spherical harmonic $Y_{\ell m}(\theta,\phi)$ can now be expressed in terms of a new coordinate system x',y',z' so chosen that $\hat{z}'$ is along $\vec{k}$. The new coordinate system is derived from the old by rotations through Euler angles ($\alpha = \phi_k$, $\beta = \theta_k$, $\gamma = 0$). The rotation matrices $D^{\ell}_{m'm}(\alpha,\beta,\gamma)$ relate $Y_{\ell m}(\theta,\phi)$ to the rotated $Y_{\ell m}(\theta',\phi')$ according to

$$Y_{\ell m}(\theta,\phi) = \sum_{m'} D^{\ell *}_{mm'}(\phi_k,\theta_k,0)Y_{\ell m'}(\theta',\phi'). \qquad \text{(D-6)}$$

Rewriting Eq. (D-5) in terms of the new variables and performing the integral over ϕ' results in

$$\begin{aligned}\chi(\ell,m,\vec{k},r) &= 2\pi\, D^{\ell *}_{mo}(\phi_k,\theta_k,0)\left[\frac{2\ell+1}{4\pi}\right]^{\frac{1}{2}} \\ &\quad \times \int_0^{\pi} P_{\ell}(\cos\theta')e^{-ikr\cos\theta'}\sin\theta'd\theta' \\ &= 2\pi\, Y_{\ell m}(\theta_k,\phi_k) \\ &\quad \times \int_0^{\pi} P_{\ell}(\cos\theta')e^{-ikr\cos\theta'}\sin\theta'd\theta' \,. \qquad \text{(D-7)}\end{aligned}$$

From Gegenbauer's generalization of Poisson's integral given by

$$J_n(z) = \tfrac{1}{2}(-i)^n \int_0^{\pi} P_n(\cos\theta)e^{iz\cos\theta}\sin\theta\, d\theta,$$

the previous equation becomes

$$\chi(\ell,m,\vec{k},\vec{r}) = 4\pi(-i)^n J_\ell(kr)\, Y_{\ell m}(\theta_k,\phi_k) \qquad \text{(D-8)}$$

Using this general result along with the functional form given in Eq. (D-2) results in the reduction of Eq. (D-4) into the final integral equation

$$\begin{aligned}\rho^\lambda(\vec{K}_\mu) = {} & \frac{8\pi}{\Omega}\cos \vec{K}_\mu\cdot\vec{t}_1 \sum_{\ell=2n}{}' (-1)^{\ell/2} \sum_m C_\ell^m Y_{\ell m}(\theta_k,\phi_k) \\ & \times \int_o^\infty g_\ell^\lambda(r)\, J_\ell(K_\mu r) r^2 dr \\ & + \frac{8\pi}{\Omega}\sin \vec{K}_\mu\cdot\vec{t}_1 \sum_{\ell=2n+1}{}' (-1)^{\frac{\ell+1}{2}} \sum_m C_\ell^m Y_{\ell m}(\theta_k,\phi_k) \\ & \times \int_o^\infty g_\ell^\lambda(r)\, J_\ell(K_\mu r) r^2 dr, \end{aligned} \qquad \text{(D-9)}$$

where $\sum_{\ell=2n}{}'$ ($\sum_{\ell=2n+1}{}'$) is a sum of even (odd) values of ℓ.

APPENDIX E

FOURIER ANALYSIS OF CHARGE DENSITY

Using the notation introduced in Chapter II, the wavefunctions can be written

$$\psi_{n,i}(\vec{k},\vec{r}) = \eta^{-\frac{1}{2}} \sum_{\nu} e^{i\vec{k}\cdot\vec{R}_\nu} \xi_{n,i}(\vec{k},\vec{r}-\vec{R}_\nu), \tag{E-1}$$

with orthonormality requirement

$$\int \psi^*_{n,i}(\vec{k},\vec{r})\psi_{n',i'}(\vec{k},\vec{r})d\tau_r = \delta_{nn'}\,\delta_{ii'}\,. \tag{E-2}$$

The contribution to electronic charge density due to the nth band and ith root for point $\vec{k}$ in the Brillouin zone is given by

$$\rho_{n,i}(\vec{k},\vec{r}) = \psi^*_{n,i}(\vec{k},\vec{r})\,\psi_{n,i}(\vec{k},\vec{r}). \tag{E-3}$$

Rewriting the wavefunctions in momentum representation results in the expression

$$\psi_{n,i}(\vec{k},\vec{K}) = (2\pi)^{-3/2} \int \psi_{n,i}(\vec{k},\vec{r})e^{-i\vec{K}\cdot\vec{r}}\, d\tau_r \tag{E-4}$$

and the reciprocal relation is given by

$$\psi_{n,i}(\vec{k},\vec{r}) = (2\pi)^{-3/2} \int \psi_{n,i}(\vec{k},\vec{K})e^{i\vec{K}\cdot\vec{r}}\, d^3K. \tag{E-5}$$

In a similar manner, the momentum representation of Eq. (E-3) is given

by

$$\rho_{n,i}(\vec{k},\vec{K}) = \frac{1}{\eta\Omega}\int_{\eta\Omega}\rho_{n,i}(\vec{k},\vec{r})e^{-i\vec{K}\cdot\vec{r}}\,d\tau_r \ . \qquad \text{(E-6)}$$

It is easy to show that substituting the form of $\rho_{n,i}(\vec{k},\vec{r})$ given by Eq. (E-3) into Eq. (E-6) and using Eq. (E-4) and Eq. (E-5) results in the following expression

$$\rho_{n,i}(\vec{k},\vec{K}') = \frac{1}{\eta\Omega}\int \psi^*_{n,i}(\vec{k},\vec{K})\ \psi_{n,i}(\vec{k},\vec{K}'+\vec{K})\,d^3K \ . \qquad \text{(E-7)}$$

A very useful expression for $\psi_{n,i}(k,\vec{K})$ is derived by substituting Eq. (E-1) into Eq. (E-4) and performing the integration. The result of this evaluation is written as

$$\psi_{n,i}(\vec{k},\vec{K}) = \eta^{-\frac{1}{2}}\,\Omega_k\,\xi_{n,i}(\vec{k},\vec{K})\sum_{\nu}\delta(\vec{k}-\vec{K}-\vec{K}_\nu), \qquad \text{(E-8)}$$

where

$$\xi_{n,i}(\vec{k},\vec{K}) = (2\pi)^{-3/2}\int \xi_{n,i}(\vec{k},\vec{r})e^{-i\vec{K}\cdot\vec{r}}\,d\tau_r \ .$$

Substituting this expression into Eq. (E-7) and performing the integration results in

$$\rho(\vec{k},\vec{K}_\mu) = \frac{\Omega_k^2}{\eta^2\Omega}\sum_{\nu\nu'}\xi^*_{n,i}(\vec{k},\vec{k}-\vec{K}_\nu)\ \xi_{n,i}(\vec{k},\vec{k}-(\vec{K}_\nu-\vec{K}_{\nu'}))\ x\ \delta(\vec{K}_\nu-K_{\nu'},-K_\mu), \qquad \text{(E-9)}$$

where $\vec{K}'$ was redefined as $\vec{K}_\mu$. Transforming the Dirac delta function in Eq. (E-9) to a Kronecker delta function and summing over ν results in the expression

$$\rho(\vec{k},\vec{K}_\mu) = \frac{\Omega_k}{\eta\Omega}\sum_{\nu'}\xi^*_{n,i}\,[\vec{k},\vec{k}-(\vec{K}_{\nu'}+\vec{K}_\mu)]\ \xi_{n,i}(\vec{k},\vec{k}-\vec{K}_{\nu'}) \ . \qquad \text{(E-10)}$$

The contribution to the Fourier coefficient of charge density due to the nth band and ith root is given by

$$\rho_{n,i}(\vec{K}_\mu) = 2\frac{\eta}{\Omega_k}\int_{BZ}\rho_{n,i}(\vec{k},\vec{K}_\mu)d\tau_k, \tag{E-11}$$

where the factor of two is due to two spin oreintations per band and $\frac{\eta}{\Omega_k}$ is the density of $\vec{k}$ points in the Brillouin zone. Transforming the integral over the Brillouin zone in Eq. (E-11) to one over the irreducible wedge and using Eq. (E-10) results in the equation

$$\rho_{n,i}(\vec{K}_\mu) = \frac{2}{\Omega}\sum_{\alpha=1}^{48}\int_{1W}\sum_{\nu}\xi^*_{n,i}(R_\alpha\vec{k}(R_\alpha\vec{k}) - (\vec{K}_\nu+\vec{K}_\mu)) \times \xi_{n,i}(R_\alpha\vec{k},$$

$$\times (R_\alpha\vec{k}) - \vec{K}_\nu)d^3k, \tag{E-12}$$

where R_α is an element of O_h. It is easily shown using Eq. (E-12) from Appendix F that the following symmetry condition holds

$$\xi_{n,i}(R_\alpha\vec{k},R_\alpha\vec{k}-\vec{K}_\nu) = e^{-iR_\alpha(\vec{k}-R_\alpha^{-1}\vec{K}_\nu)\cdot\vec{\tau}_\alpha} \times \sum_j C_{ij}^{n\alpha}(\vec{k})\xi_{n,j}(\vec{k},\vec{k}-R_\alpha^{-1}\vec{K}_\nu), \tag{E-13}$$

where

$$\psi_{n,i}(R_\alpha\vec{k},R_\alpha\vec{r}+\vec{\tau}_\alpha) = \sum_j C_{ij}^{n\alpha}(\vec{k})\ \psi_{n,j}(\vec{k},\vec{r}),$$

and where $C^{n\alpha}(\vec{k})$ is a unitary transformationmatrix for which

$$\sum_i C^n_{ij}(\vec{k})\ C^n_{ij'}(\vec{k}) = \delta_{ij},$$

The final expression for the contribution to $\rho(\vec{K}_\mu)$ for the nth band is found by substituting the symmetry relation given in Eq. (E-13)

into Eq. (E-12) and summing over the roots i. This final result is written as

$$\rho_n(\vec{K}_\mu) = \frac{2}{\Omega} \sum_\alpha \sum_j \sum_\nu \int_{1W} e^{i(R_\alpha \vec{K}_\mu)\cdot\vec{\tau}_\alpha} \xi^*_{n,j}(\vec{k},\vec{k}-R_\alpha(\vec{K}_\nu+\vec{K}_\mu))$$

$$\times \xi_{n,j}(\vec{k},\vec{k}-R_\alpha\vec{K}_\nu)d^3k \ . \qquad \text{(E-14)}$$

APPENDIX F

COMPTON PROFILE

Using the notation introduced in Chapter II, the wavefunctions can be written

$$\psi_n(\vec{k},\vec{r}) = \eta^{-\frac{1}{2}} \sum_{\nu} e^{i\vec{k}\cdot\vec{R}_\nu} \xi_n(\vec{k},\vec{r}-\vec{R}_\nu), \tag{F-1}$$

with the orthonormality requirement

$$\int \psi_n^*(\vec{k},\vec{r})\ \psi_{n'}(\vec{k},\vec{r})d\tau_r = \delta_{nn'}. \tag{F-2}$$

The momentum representation of the wavefunction $\psi_{n,i}(k,\vec{K})$ is given by

$$\psi_n(\vec{k},\vec{K}) = (2\pi)^{-3/2} \int \psi_n(\vec{k},\vec{r})e^{-i\vec{K}\cdot\vec{r}}\, d\tau_r . \tag{F-3}$$

Using the results of Eq. (E-8) from Appendix E, this expression is written as

$$\psi_n(\vec{k},\vec{K}) = \eta^{-\frac{1}{2}}\, \Omega_k\, \xi_n(\vec{k},\vec{K}) \sum_{\nu} \delta(\vec{k}-\vec{K}-\vec{K}_\nu), \tag{F-4}$$

where

$$\xi_n(\vec{k},\vec{K}) = (2\pi)^{-3/2} \int \xi_n(\vec{k},\vec{r})e^{-i\vec{K}\cdot\vec{r}}\, d\tau_r .$$

The contribution to the momentum density from nth band for a particular $\vec{k}$ point in the Brillouin zone given by

$$\rho_n(\vec{k},\vec{K}) = \psi_n^*(\vec{k},\vec{K})\ \psi_n(\vec{k},\vec{K}). \qquad \text{(F-5)}$$

It is straightforward to show that substituting Eq. (F-4) into Eq. (F-5) results in the expression

$$\rho_n(\vec{k},\vec{K}) = \Omega_k \left|\xi_n(\vec{k},\vec{K})\right|^2 \times \sum_\nu \delta(\vec{k}-\vec{K}-\vec{K}_\nu) \ . \qquad \text{(F-6)}$$

The momentum density per unit atom for filled band n can be expressed

$$\rho_n(\vec{K}) = \frac{\eta}{\Omega_k} \int_{BZ} \rho_n(\vec{k},\vec{K})\ d\tau_{k/\eta} \ , \qquad \text{(F-7)}$$

where $\frac{\eta}{\Omega_k}$ is the density of $\vec{k}$ points in the Brillouin zone and $1/\eta$ normalizes the momentum density to one atom. Substituting Eq. (F-6) into Eq. (F-7) and integrating over the Brillouin zone results in the equation

$$\rho_n(\vec{K}) = \left|\xi_n(\vec{K}+\vec{K}_\alpha,\vec{K})\right|^2 \ , \qquad \text{(F-8)}$$

where $\vec{K}_\alpha$ is a reciprocal lattice vector for which $\vec{K} + \vec{K}_\alpha$ lies in the Brillouin zone. Rewriting Eq. (F-8) with the understanding that the first argument is to be expressed in the reduced zone scheme results in the simple expression for momentum density

$$\rho_n(\vec{K}) = \left|\xi_n(\vec{K},\vec{K})\right|^2 \ . \qquad \text{(F-9)}$$

The wavefunction must obey the following symmetry relation

$$\psi_{n,i}(R_\gamma \vec{k}, R_\gamma \vec{r}+\vec{\tau}_\gamma) = \sum_j C_{ij}^{n\gamma}(\vec{k})\ \psi_{n,j}(\vec{k},\vec{r}), \qquad \text{(F-10)}$$

where R_γ is an element of O_h and $C^n(\vec{k})$ is a unitary transformation matrix. A similar relation can be derived for the momentum representation of $\psi_{n,i}(\vec{k},\vec{r})$ by first rewriting Eq. (F-3) in the form

$$\psi_{n,i}(R_\gamma \vec{k}, R_\gamma \vec{K}) = (2\pi)^{-3/2} \int \psi_{n,i}(R_\gamma \vec{k},\vec{r})\ e^{-iR_\gamma \vec{K}\cdot\vec{r}}\ d\tau_r,$$

then transforming the variable of integration $\vec{r}$ to the new coordinates $R_\gamma \vec{r}'+\vec{\tau}_\gamma$ and making explicit use of Eq. (F-10).

The resulting expression is written as

$$\psi_{n,i}(R_\gamma \vec{k}, R_\gamma \vec{K}) = e^{-iR_\gamma \vec{K}\cdot\vec{\tau}_\gamma} \sum_j C_{ij}^{n\gamma}(\vec{k})\ \psi_{n,j}(\vec{k},\vec{K}). \qquad \text{(F-11)}$$

Substituting Eq. (F-4) into both sides of Eq. (F-11) and collecting terms results in the equation

$$\xi_{n,i}(R_\gamma \vec{k}, R_\gamma \vec{K}) = e^{-iR_\gamma \vec{K}\cdot\vec{\tau}_\gamma} \sum_j C_{ij}^{n\gamma}(\vec{k})\ \xi_{n,j}(\vec{k},\vec{K}). \qquad \text{(F-12)}$$

Using the symmetry relationship given by Eq. (F-12), the momentum density given in Eq. (F-9) yields the relation

$$\rho(R_\gamma \vec{K}) = \rho(\vec{K})\ . \qquad \text{(F-13)}$$

Within the impulse approximation, the Compton profile $J(q,\hat{k})$ is related to the band states by the expression

$$J(q,\hat{k}) = \int \delta(q-\hat{k}\cdot\vec{K})\ \rho(\vec{K})\ d^3K\ . \qquad \text{(F-14)}$$

The integral over reciprocal space in Eq. (F-14) can be re-expressed as a sum of integrals over the Brillouin zone having the form

$$J(q,\hat{k}) = \sum_{\mu} \int_{\Omega_k} \delta(q-\hat{k}\cdot(\vec{k}+\vec{K}_{\mu})) \; \rho(\vec{k}+\vec{K}_{\mu}) \; d^3k \; . \qquad \text{(F-15)}$$

Combining Eq. (F-13) and Eq. (F-15) permits the Compton profile to be further reduced to an integration over the irreducible wedge of the form

$$J(q,\hat{k}) = \sum_{\mu} \sum_{\gamma} \int_{1W} \delta(q-(R_{\gamma}\hat{k})\cdot(\vec{k}+\vec{K}_{\mu})) \; x \; \rho(\vec{k}+\vec{K}_{\mu}) \; d^3k \; . \qquad \text{(F-16)}$$

VITA[2]

Richard Alan Heaton

Candidate for the Degree of

Doctor of Philosophy

Thesis: A THEORETICAL INVESTIGATION OF THE ELECTRONIC BAND STRUCTURE AND BULK PROPERTIES OF DIAMOND

Major Field: Physics

Biographical:

Personal Data: Born in Wichita, Kansas, July 19, 1948, the son of Richard R. and Esther L. Heaton; married Irene L. Kleim, December 12, 1975; have one daughter, Rachel, born April 20, 1978.

Education: Graduated from Northwest Classen High School, Oklahoma City, Oklahoma, in May, 1966; received Bachelor of Science degree in physics from Oklahoma State University in December, 1972; completed requirements for Doctor of Philosophy degree at Oklahoma State University, May, 1979.

Professional Experience: Graduate Research Assistant, Physics Department, Oklahoma State University, 1973; Graduate Teaching Assistant, Physics Department, Oklahoma State University, 1974-78; Visiting Scientist, I.B.M. Research Labs, San Jose, California, summer, 1977; Research Associate, University of Wisconsin, Madison, Wisconsin, 1978.